TÜBİTAK

Turkish Journal of Chemistry

http://journals.tubitak.gov.tr/chem/

Research Article

Turk J Chem
(2017) 41: 309 – 322

doi:10.3906/kim-1603-15

Synthesis and photovoltaic characterization of triarylamine-substituted quinoxaline push–pull dyes to improve the performance of dye-sensitized solar cells

Kadir DEMİRAK[1], Mustafa CAN[2], Cihan ÖZSOY[1], Mesude Zeliha YİĞİT[2], Burak GÜLTEKİN[1], Şerafettin DEMİÇ[3], Ceylan ZAFER[1,*]

[1]Solar Energy Institute, Ege University, İzmir, Turkey

[2]Department of Engineering Sciences, Faculty of Engineering and Architecture, İzmir Katip Çelebi University, İzmir, Turkey

[3]Department of Materials Science and Engineering, Faculty of Engineering and Architecture, İzmir Katip Çelebi University, İzmir, Turkey

Received: 07.03.2016 • **Accepted/Published Online:** 03.02.2017 • **Final Version:** 16.06.2017

Abstract: Novel unsymmetrical organic sensitizers having donor, π-spacer, and anchoring groups were designed and synthesized for dye-sensitized solar cell (DSSC) application. The dyes 3-{4-[7-(4-{bis[4-(hexyl)phenyl]amino} phenyl)-11,12-dibutoxy-1,4,5,8-tetrahydrodibenzo [a, c] phenazine-2-yl]phenyl} -2-cyano acrylic acid (KD-148) and 3-{5-[7-(4-{bis[4-(hexyloxy)phenyl]amino} phenyl)-11,12-dibutoxy-1,4,5,8-tetrahydrodibenzo [a, c] phenazine-2-yl]-2-thienyl} -2-cyano acrylic acid (KD-150) were anchored onto TiO_2 and tested with ionic liquid electrolyte. The monochromatic incident photon-to-current conversion efficiencies (IPCE) of the dyes were 50% and 60% at 420 nm, respectively. The KD-150–sensitized solar cell gave a short-circuit current (I_{SC}) of 7.37 mA/cm^2, an open-circuit voltage (V_{oc}) of 560 mV, a fill factor (FF) of 0.56, and overall conversion efficiency (η) of 2.32% whereas the standard dye Z-907 dye exhibited 14.51 mA/cm^2 of I_{SC}, 630 mV of V_{oc}, 0.45 of FF, and 4.08% of η under AM 1.5 illumination with power of 100 mW/cm^2.

Key words: Dye-sensitized solar cells, photovoltaics, push–pull dyes, quinoxaline dyes

1. Introduction

Dye-sensitized solar cells (DSSCs) have attracted increasing attention as low-cost alternatives to conventional semiconductor photovoltaic devices.[1,2] It is also important to note that the production of DSSCs' key materials is an environmentally friendly and energy saving process in contrast to the traditional silicon technology. DSSCs are composed of a wide band gap nano-crystalline semiconductor oxide like TiO_2 deposited on a transparent conductive oxide (TCO)-coated glass substrate and sensitized with a dye absorbing visible light. On the basis of material design and device engineering, remarkable efficiencies of 12% and 13% have been achieved from DSSCs sensitized with ruthenium[3] and zinc porphyrin dyes,[4] respectively. On the other hand, the tunable structure, high molar extinction coefficient, low production cost, easier synthetic procedure, purification, and low toxicity of all organic dyes make them more suitable candidates for DSSC applications. Thus, a great number of studies have focused on energy-level engineering of chromophores such as indoline,[5,6] diketopyrollopyrrole,[7]

*Correspondence: ceylan.zafer@ege.edu.tr

triarylamine,[8,9] iminocoumarin,[10] carbazole,[11,12] perylene,[13] and many other derivatives in order to enhance light harvesting on the metal oxide surface by adding various side chains, arranging the length of the π-bridge groups, or using acceptor and donor groups with different electron affinities.

Furthermore, these dyestuffs need to be controllably grafted onto the inorganic mesoporous semiconductor oxide film with favorable stacking modes and optimum energy alignments and have a significant effect on charge-transfer kinetics to obtain remarkably high cell efficiencies.[3]

Donor-π-bridge-acceptor (D-π-A) block structure is the most common configuration in order to obtain high charge separation rate on the organic sensitizer. In a well-designed D-π-A molecule, intramolecular charge transfer (ICT) occurs efficiently between the donor and the acceptor parts of the dye. As a modification of this strategy, some new donor-acceptor-π-acceptor (D-A-π-A) organic dyes have been synthesized by adding an internal electron-withdrawing unit such as benzothiadiazole, benzotriazole, diketopyrrolopyrrole, and quinoxaline to the traditional D-π-A structure to extend further the spectral response.[14]

We report two new organic sensitizers for DSSCs with different chemical structures comprising different functional groups and try to make a comparison between the two structures from the point of view of charge injection abilities depending on two different pi-bridges, phenyl and thiophene. Many parameters such as light absorption, charge injection, $\pi-\pi$ interaction, and recombination were taken into consideration during the design of the structures of the molecules and synthesis. Therefore, D-A-π-A structure was chosen for the best performance.

Two new D-A-π-A type metal-free sensitizers (KD-148 and KD-150) were designed and synthesized. 11,12-Dibutoxydibenzo [a,c] phenazine was used as acceptor (A) between donor and π-spacer groups in order to enhance the diffusion of the generated charges on the donor part of the dyes. Beside this, butoxy groups on the A', phenazine were used to decrease the intermolecular energy transfer between sensitizer molecules. Furthermore, two different types of π-spacers, thiophene (KD-150) and benzene (KD-148) were used to investigate the charge transfer properties of those moieties on the photovoltaic performance of the corresponded dyes. Here, the photovoltaic performances of KD-148 and KD-150 sensitizers in DSSC applications are reported under standard conditions. The molecular structures of KD-148 and KD-150 dyes are presented in Figure 1.

2. Results and discussion

2.1. Synthesis and structural characterization

The synthetic route of the dyes is given in the Scheme. In the first part of the synthesis, 1,2-dibutoxybenzene (**2**) was prepared from commercial catechol and 1-iodobutane via Williamson etherification in acetone in the presence of base[15] after nitration;[16] 1,2-dibutoxy-4,5-dinitrobenzene (**3**) was reduced to the diamine compound (**4**),[17] said to be sensitive to air, and directly reacted with 2,7-dibromo-phenantrene-9,10-dion by an acid-catalyzed dehydration reaction[18] to get the π-spacer (**5**). In the second part of the synthesis, 1-(hexyloxy)-4-iodophenol (**7**) was synthesized via Williamson etherification[6] and reacted with 4-bromoaniline via the Ullmann reaction using copper (I) iodide and 1,10-phenantroline as catalyst in toluene in the presence of base at 120 °C to obtain triarylamine derivative (**8**). (4-{Bis[4-(hexyloxy)phenyl]amino} phenyl) boronic acid (**9**) was synthesized using n-BuLi in dry THF at –80 °C and the lithiated compound was reacted with trimethylborate to give boronic acid derivative. In the last part of the synthesis, π-spacer (**5**) and boronic acid compound (**9**) were reacted and 4-formyl phenyl boronic acid and 2-tienyl boronic acid were attached to compound **10** via Suzuki coupling in the

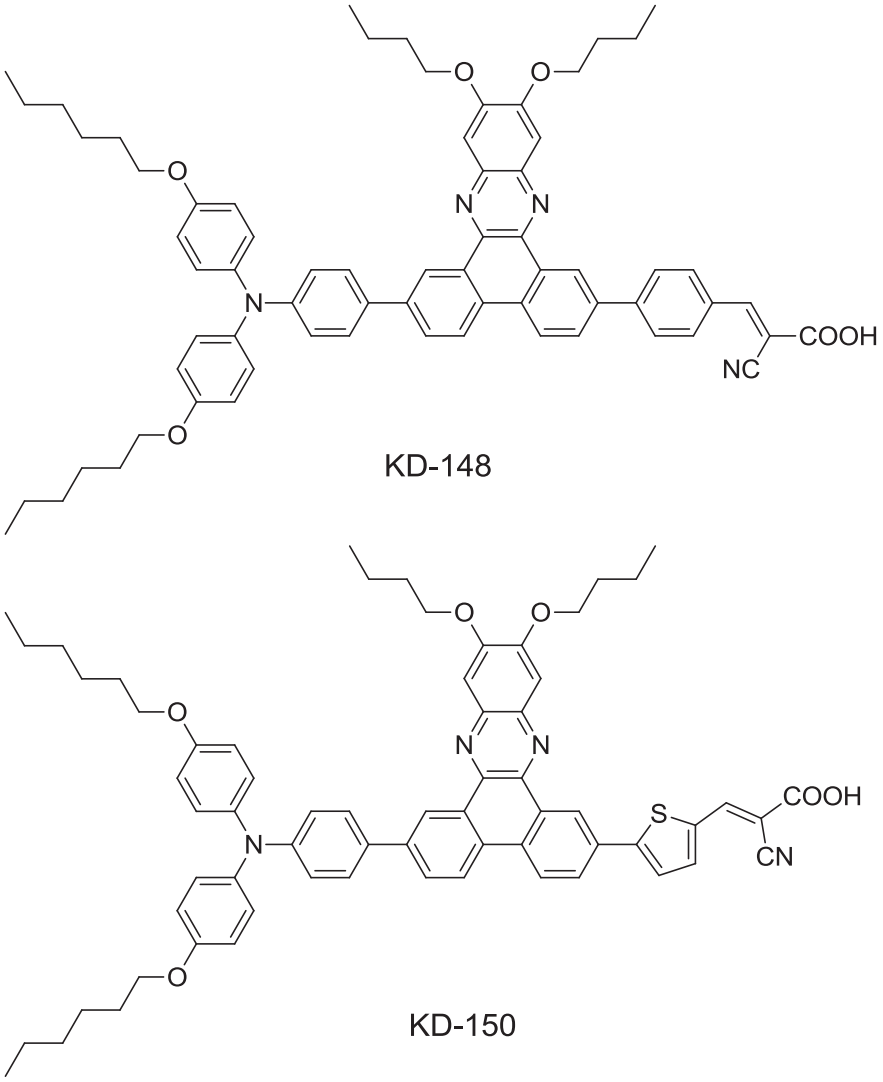

Figure 1. The molecular structure KD-148 and KD-150.

presence of palladium catalyst. These reagents (**11**, **12**) were condensed with cyanoacrylic acid via Knoevenagel condensation reactions in the presence of piperidine to result in the formation of the final dyes KD-148 and KD-150. All intermediates were confirmed by ^{1}H and ^{13}C NMR.

2.2. Electrochemical properties

Energy levels of dye sensitizers are crucial to understand and investigate the ability of electron transfer and the molecular orbital energy levels. Regarding this, cyclic voltammetry (CV) analysis was employed to determine the redox potentials of the dyes in liquid phase. Representative cyclic voltammograms are shown in Figure 2. Generally, triarylamine groups give an oxidation signal at around 1.2 V. However, the presence of an alkoxy chain in the triarylamine structure shifts the oxidation potential anodically to around 1.0 V. This shift results from the donation of the unpaired electron of oxygen to the system. In addition, by considering the structure of triarylamine groups, a second oxidation signal might be observed. As seen in Figure 2, the reversible oxidation

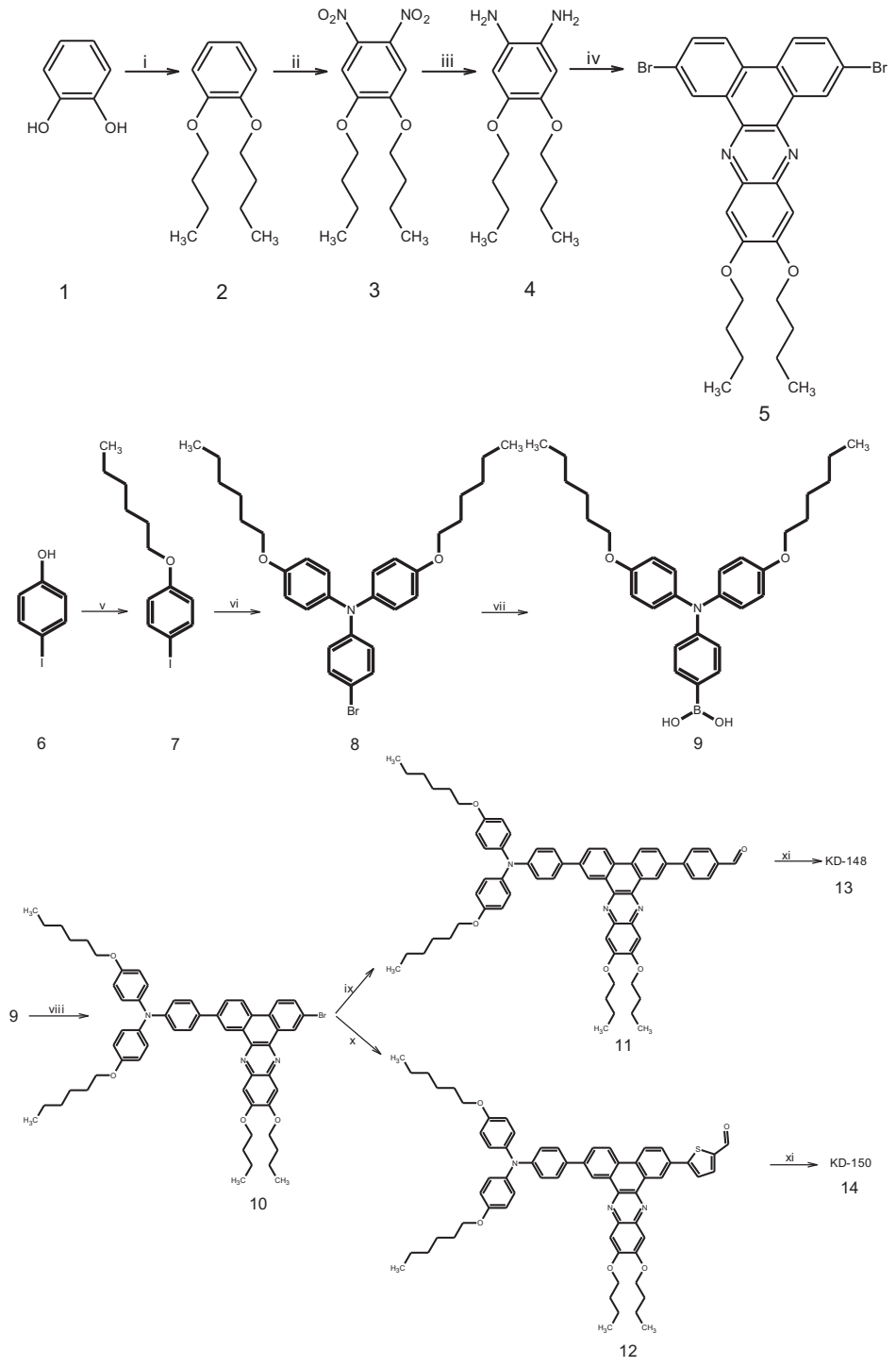

Scheme. Synthetic route of KD-148 and KD-150. Reagents: (i) 1-iodobutane, K_2CO_3, acetone; (ii) HNO_3, acetic acid, CH_2Cl_2; (iii) PdC (10%), hydrazine hydrate, EtOH; (iv) 2,7-dibromo-phenantrene-9,10-dion, acetic acid, toluene; (v) 1-bromohexane, K_2CO_3, 18-crown-6, acetone; (vi) 4-bromo aniline, CuI, 1,10-phenantroline, KOH, toluene; (vii) *n*-BuLi, $B(OMe)_3$, THF; (viii) 2, 7-Dibromo-11,12-dibutoxydibenzo [a, c] phenazine, Pd(dppf)Cl_2, DME, K_2CO_3 (aq); (ix) 4-formyl phenyl boronic acid, Pd(dppf)Cl_2, DME, K_2CO_3 (aq); (x) 5-formyl-2-tienylboronic acid, Pd(dppf)Cl_2, DME, K_2CO_3 (aq); (xi) 2-cyanoacetic acid, piperidine, $CHCl_3$.

potentials of dyes are observed at around 0.8–0.9 V attributed to the alkoxy-substituted tripheylamine derivative. Moreover, in the reduction part of the voltammograms, the cyanoacrylic acid moiety of each molecule exhibits an irreversible peak.

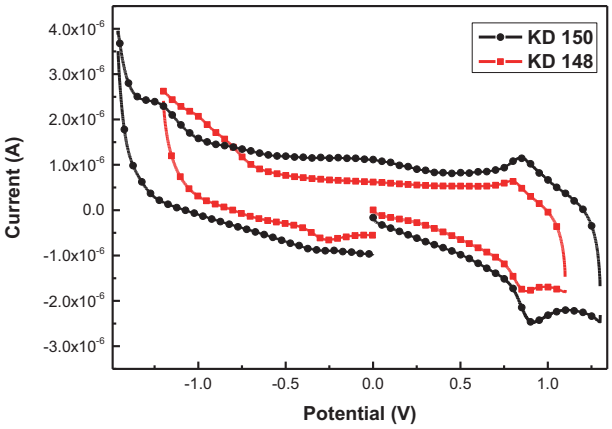

Figure 2. Cyclic voltammograms of KD-148 and KD-150 in chloroform.

Reduction peaks of cyanoacrylic acid on both KD-148 and KD-150 shifted to higher negative potential due to the weak acceptor behavior of the π-spacer, quinoxaline.

As depicted in Figure 2, KD-150 has an irreversible peak at higher voltage value compared to KD-148 and this observation is attributed to the structures of the dyes. KD-150 has a thiophene unit on the backbone of the dye molecule and its presence extends the conjugation and makes the unpaired electron of sulfur available for donation as well. Therefore, these two positive effects supplied by the thiophene unit, compared to KD-148, which has a phenyl group, leads to the observation of an extra reduction signal in the negative part of the voltammogram.

The excitation energies (E_{0-0}) were roughly determined as 1.62 eV and 1.98 eV for KD-148 and KD-150, respectively, as given in Table 1. The HOMO and LUMO values versus vacuum were calculated by the equation

Table 1. Spectral and electrochemical properties of KD-148 and KD-150 dyes.

Dye	λ_{abs}*	E	E_G	E_{ox}	E_{red}	E_{LUMO}	E_{HOMO}
	(nm)	(M^{-1} cm^{-1})	(eV)	(V)	(V)	(eV)	(eV)
KD-148	417	65,300	1.62	0.72	–0.9	–3.50	–5.12
KD-150	415	66,900	1.98	0.78	–1.2	–3.20	–5.18

$$E_{\mathrm{LUMO/HOMO}}, e(4.88 + V_{\mathrm{redox}}),$$

where V_{redox} is the onset potential versus ferrocene of reduction or oxidization of sensitizers. The LUMO levels of the dyes KD-148 and KD-150 are –3.50 eV and –3.20 eV vs. vacuum, respectively. LUMO levels of these dyes are reasonably suitable to provide a sufficient thermodynamic driving force for electron injection from their excited states to the conduction band of TiO_2.[19] The HOMO levels of KD-148 and KD-150 are –5.12 eV and –5.18 eV vs. vacuum, respectively, and these values are also suitable for dye regeneration by redox couple (I^-/I_3^-).

2.3. Photophysical properties

As presented in Figure 3, the electronic absorption spectra of KD-148 and KD-150 in $CHCl_3$ (1×10^{-5} M) were measured for a preliminary evaluation of their light-harvesting capacities in certain concentrations. The molar extinction coefficients (ε) of KD-148 and KD-150 in $CHCl_3$ are 65,300 and 66,900 at 420 nm, respectively. In the visible region, both dyes gave an absorption peak assigned to $n-\pi^*$ transition. The absorption peak of KD-150 exhibits a considerable bathochromic shift compared to KD-148. This result clearly illustrates that thiophene moiety in KD-150 leads to more conjugation in its molecular structure. Furthermore, it is known that thiophene has a lower aromaticity as compared to benzene[20,21] because of its smaller stabilization energy (thiophene 19 kcal/mol; benzene 36 kcal/mol), which allows better electron delocalization as reported by March.[22]

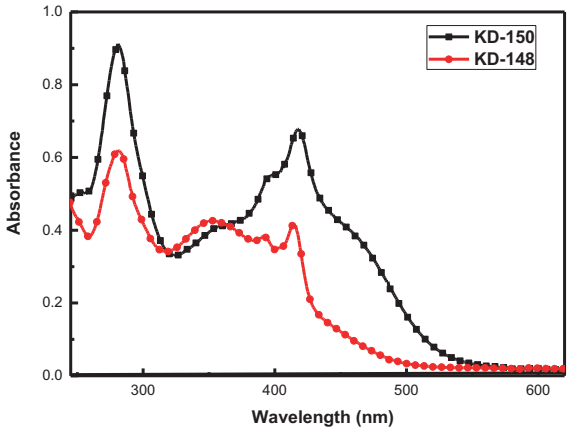

Figure 3. Absorption curves of KD-148 and KD-150 in chloroform.

KD-148 and KD-150 exhibit significantly improved light absorption coefficients, ensuring good light absorption even if a thin active layer is used for efficient device operation.[23] Moreover, a reduction in film thickness can improve the open-circuit voltage obtained from the solar cell device.

2.4. Photovoltaic performance of DSSCs

The photovoltaic characterizations of these dyes were measured with a sandwich geometry type of photovoltaic cell using a liquid redox electrolyte. Figure 4 depicts the IPCE as a function of the wavelength for the cells. The IPCE maximum for KD-148 and KD-150 sensitized DSSCs is around 50% and 60% at 420 nm, respectively. The IPCE spectrum of KD-150 is broader (300 nm to 600 nm) than that of KD-148 (300 nm to 550 nm), which is consistent with the absorption spectra of the sensitizers. Furthermore, due to the better electron transport property of thiophene moiety than that of benzene, KD-150 has a higher photon to current conversion efficiency. On the other hand, the IPCE data proved that the light in the absorption range of both dyes can be mostly converted to photocurrent. It is valuable to note that the IPCE spectra of both dyes are in the range between the UV and visible region of the solar spectrum, highlighting the necessity of further efforts on narrowing the band gap of metal-free organic dyes in order to shift the absorption band to the visible and near infrared region.

The current density–voltage (J–V) characteristics of DSSCs based on KD dyes are shown in Figure 5 and listed in Table 2. The J–V curves were measured under irradiation conditions of AM 1.5 G. Both solar cells fabricated with KD-148 and KD-150 have an active area of 1 cm^2. The short-circuit photocurrent (I_{SC}), open-circuit photovoltage (V_{oc}), and fill factor (FF) parameters of KD-148 and KD-150 sensitized cells are

4.92 mA/cm^2, 520 mV, and 0.6 and 7.37 mA/cm^2, 560 mV, and 0.56, yielding overall conversion efficiencies (η) of 1.54% and 2.32%, respectively (Table 2), while the photovoltaic parameters of the standard cell with Z-907 dye are 14.51 mA/cm^2, 630 mV, and 0.45 with a power conversion efficiency of 4.08%. In contrast to cell efficiencies, KD-148 and KD-150 dyes have fill factors better than that of Z-907. The yields and results can be explained by differences in the structural properties of the dyes. The thiophene group of KD-150 contains a sulfur atom with two nonbonded electron pairs. These electrons increase the absorption intensity and exhibit a broader absorption spectrum through the IR region as seen in Figure 4, leading to the increase in the number of generated charge carriers contributing to a higher short-circuit current.

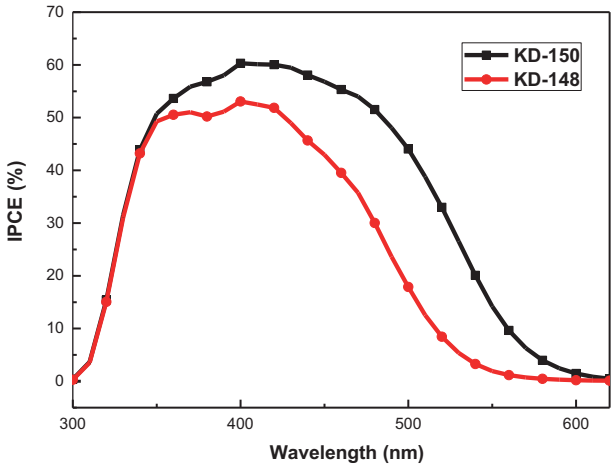

Figure 4. IPCE curves of KD-148 and KD-150.

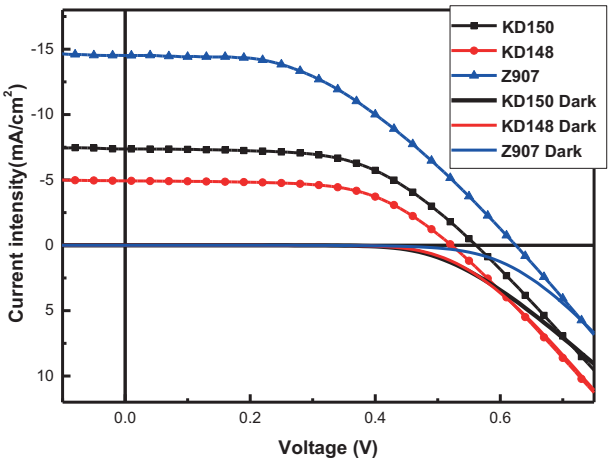

Figure 5. J-V curves of KD-148, KD-150 and reference dye Z-907.

Table 2. Photovoltaic performance of the DSSCs sensitized with KD-148, KD-150, and reference dye Z-907 under 100 mW cm^{-2} light intensity and AM 1.5 global radiation.

Dye	I_{sc} (mA/cm^2)	V_{oc} (mV)	FF	M. power (mA/cm^2)	I_{mpp} (mA/cm^2)	V_{mpp} (mV)	η (%)
KD-148	4.92	520	0.60	1.54	4.16	370	1.54
KD-150	7.37	560	0.56	2.32	6.28	370	2.32
Z-907	14.51	630	0.45	4.08	11.34	360	4.08

There are several contributing factors to IPCE and J_{SC} of a DSSC in connection with the sensitizer. The primary one is the molar extinction coefficient (ε) and the secondary one is the charge injection rate. To consider them together, the enhanced light absorption and charge injection arising from π-bridge lengthening should boost the light capture and charge separation, respectively, resulting in increased IPCE and J_{SC} and alleviated charge recombination.[24] Regarding this statement, KD-150 has better photocurrent generation efficiency (IPCE) values compared to KD-148 and a similar trend was observed in J_{SC}. Furthermore, length of the alkoxy chains substituted to the backbone of dyes affects the interaction between the dye molecule and the electrolyte. $\pi-\pi$ interactions in planar groups such as quinoxaline π-bridge are strong enough to form aggregates in solution and also at the surface of the TiO_2 mesoporous network. Aggregation of the sensitizers increases the recombination ratio of injected electrons from TiO_2 conduction to the HOMO level of the sensitizer or to the redox couple in the electrolyte.[25–27]

3. Experimental

3.1. Materials

All solvents and reagents, unless otherwise stated, were of puriss quality and used as received. Catechol, copper (I) iodide, and 1-bromohexane were purchased from Fluka. 1-Iodobutane, acetone, nitric acid, dichloromethane, ethanol, toluene, phenantrene-9, 10-dion, 18–crown-6, 1,10-phenantroline, $n-$butyllithium, 1,2-dimethoxyethane, tetrahydrofuran, trimethyl borate, and [1,1'-bis(diphenylphospino)ferrocene] dichloropalladium(II) were obtained from Sigma-Aldrich. 4-Iodophenol and 4-bromoaniline were from Alfa Aesar. Potassium carbonate and potassium hydroxide were purchased from Riedel de Haen and hydrazine hydrate and palladium activated carbon from Merck.

3.2. Synthetic procedures

Synthesis of 1,2-dibutoxybenzene (**2**): A mixture of catechol (8.8 g, 80 mmol), 1-iodobutane (18 mL, 160 mmol), potassium carbonate (26 g, 160 mmol), and acetone (80 mL) were refluxed with stirring in a round bottomed flask for 2 days. Reaction progress was monitored by thin layer chromatography (TLC). After cooling the reaction mixture it was filtered and washed with pure acetone. The final solution was extracted with water (2 $\times$ 30 mL) and dichloromethane (2 $\times$ 30 mL). The organic phase was separated, washed with 1 M hydrochloric acid, and dried over sodium sulfate. The organic solvents were evaporated by rotary evaporator under vacuum and the crude product purified by column chromatography (toluene) on silica gel to yield colorless oil (88% yields). ^{1}H NMR (400 MHz d_6-DMSO): δ 6.93 (m, $J=$ 4 Hz, 4H), 4.04 (t, $J=$ 8 Hz, 4H), 1.88–1.81 (m, 4H), 1.60–1.51 (m, 4H), 1.03 (t, $J=$ 8 Hz, 6H).

Synthesis of 1,2-dibutoxy-4,5-dinitrobenzene (**3**): In a round bottomed flask 1,2-dibutoxybenzene (4.5 g, 20 mmol), acetic acid (140 mL), and dichloromethane (140 mL) were mixed. To this mixture was added dropwise nitric acid 65% (20 mL), followed by stirring for 30 min. Then fuming nitric acid 100% (50 mL) was added dropwise. The reaction mixture was stirred for 3 days at room temperature, and controlled and ended by TLC. The cooled reaction mixture was poured into iced-water and extracted with water (3 $\times$ 200 mL). The residue was washed with aqueous sodium bicarbonate solution (150 mL) and brine (150 mL). The organic phase was separated and evaporated by rotary evaporator. The crude product was recrystallized in acetone and water to afford yellow colored needle crystals (83% yield). ^{1}H NMR (400 MHz $CDCl_3$): δ 7.3 (s, 2H) 4.11 (t, $J=$ 8 Hz, 4H), 1.89–1.82 (m, 4H), 1.55–1.47 (m, 4H), 1.00 (t, $J=$ 8 Hz, 6H).

Synthesis of 1,2-dibutoxy-4,5-diaminobenzene (**4**). A three necked round bottomed flask and reflux condenser were set up; the system was vacuumed and flushed three times with argon to provide an isolated atmosphere. $1,2-$Dibutoxy-4,5-dinitro benzene (3.13 g, 10 mmol) was dissolved in ethanol (75 mL) and then this solution was added to the flask by syringe under argon. While the temperature was set to the boiling point, palladium activated carbon (10%) was added to the flask and its content was set to vigorous stirring. Hydrazine hydrate (20 mL) and ethanol (20 mL) mixture was added dropwise from a dropping funnel. The content was refluxed with stirring overnight, and checked and ended by TLC. The reaction mixture was filtered hot, cooled down to room temperature, and poured into iced-water to afford a white solid that showed sensitivity to air.

Synthesis of 2,7-dibromo-11,12-dibutoxydibenzo [a, c] phenazine (**5**). 1,2-Diamino-4,5-dibutoxy benzene (0.8 g, 3 mmol) was dissolved in toluene (10 mL) and added to a round bottomed flask. 2,7-Dibromophenantrene-9,10-dion (1 g, 3 mmol), acetic acid (15 mL), and toluene (10 mL) were added to the flask and

its content was refluxed with stirring overnight. Reaction progress was monitored by TLC. At the end of the reaction, the mixture was cooled to room temperature and extracted with dichloromethane (3 × 20 mL) and water (3 × 20 mL). Then the organic phase was dried over magnesium sulfate and evaporated by rotary evaporator. The crude product was purified by column chromatography (dichloromethane/hexane, 4/1, v/v) on silica gel to afford a yellow solid (92% yield). ^{1}H NMR (400 MHz, $CDCl_3$): δ 9.13 (d, J = 4 Hz, 2H), 8.09 (d, J = 8 Hz, 2H), 7.65 (dd, J_1 = 4 Hz, J_2 = 4 Hz, 2H), 7.28 (s, 2H), 4.24 (t, J = 8 Hz, 4H), 2.02–1.95 (m, 4H), 1.68–1.59 (m, 4H), 1.09 (t, J = 8 Hz, 6H).

Synthesis of 1-(hexyloxy)-4-iodophenol (**7**). In a round bottomed flask 4-iodophenol (8.8 g, 40 mmol), potassium carbonate (5.6 g, 40 mmol), 18−crown-6 (1 g, 4 mmol), acetone (100 mL), and 1-bromohexane (6.6 g, 40 mmol) were added and refluxed with stirring overnight. After checking the completion of the reaction by TLC, it was set to cooling to room temperature. Then it was filtered and extracted with diethylether (20 mL) and water (20 mL). The organic phase was separated, dried over sodium sulfate, and evaporated by rotary evaporator. The crude product was purified by column chromatography (dichloromethane/hexane: 1/1, v/v) to afford a colorless oil (91%, yield). ^{1}H NMR (400 MHz $CDCl_3$): δ 7.50 (d, J = 4 Hz, 2H), 6.63 (d, J = 8 Hz, 2H), 3.87 (t, J = 8 Hz, 2H), 1.76–1.70 (m, 2H), 1.44–1.39 (m, 2H), 1.34–1.29 (m, 4H), 0.89 (t, J = 4 Hz, 3H). ^{13}C NMR (400 MHz $CDCl_3$): δ 138.37, 117.18, 68.35, 31.84, 29.41, 25.96, 22.87, 14.30.

Synthesis of (4-bromophenyl)-bis[4-(hexyloxy)phenyl]amine (**8**). In a round bottomed flask copper (I) iodide (0.2 g, 1 mmol) and 1,10-phenantroline (0.18 g, 1 mmol) were added and dissolved in toluene (10 mL). The Dean-Stark apparatus and condenser were set and the reaction mixture was stirred under reflux for half an hour. 1-(Hexyloxy)-iodobenzene (5 g, 16 mmol), 4-bromoaniline (1.65 g, 9.6 mmol), potassium hydroxide (4.8 g, 77 mmol), and toluene (20 mL) were added to the refluxing solution. Then the whole mixture was refluxed with stirring overnight. After the completion of the reaction (by TLC), it was cooled to room temperature, filtered over Celite, and the residue was washed with dichloromethane. The liquid part was extracted with dichloromethane (3 × 20 mL) and water (3 × 20 mL). The combined organic phase was dried over sodium sulfate and evaporated by rotary evaporator. The crude product was purified by column chromatography (dichloromethane/hexane: 1/4, v/v) on silica gel to yield a yellow oil (66% yield). ^{1}H NMR (400 MHz, $CDCl_3$): δ 7.21 (d, J = 8 Hz, 2H), 7.00 (d, J = 8 Hz, 2H), 6.8 (d, J = 8 Hz, 6H), 3.91 (t, J = 4 Hz, 4H), 1.78–1.72 (m, 4H), 1.46–1.42 (m, 4H), 1.36–1.32 (m, 8H), 0.90 (t, J = 8 Hz, 6H). ^{13}C NMR (400 MHz, $CDCl_3$): δ 168.37, 134.67, 131.33, 130.50, 128.98, 127.89, 127.24, 125.16, 110.48, 40.43, 40.23, 40.02, 39.81, 39.60.

Synthesis of (4-{bis[4-(hexyloxy)phenyl]amino} phenyl)boronic acid (**9**). A round bottomed flask was evacuated and filled with argon gas to provide an inert atmosphere. (4−Bromophenyl)−bis[4-(hexyloxy)phenyl] amine (3.8 g, 7.3 mmol) was dissolved with dry THF (10 mL) and added to flask by needle; temperature was set to –80 °C with acetone and dry ice. To this solution n−butyl lithium (3.75 mL, 7.25 mmol) was added carefully in a dropwise manner and the whole solution was stirred for half an hour. Trimethylborate (8.4 mL, 72.6 mmol) was added in the same manner as for n-butyl lithium. The reaction progress was monitored by TLC control. Then the residue was mixed with 1 M hydrochloric acid aqueous solution (3 × 30 mL) and extracted with diethyl ether (3 × 30 mL). The organic phase was separated, dried over sodium sulfate, and evaporated by rotary evaporator. The crude product was purified by column chromatography (ethyl acetate/hexane: 3/1, v/v) on silica gel to afford a white solid (74% yield). ^{1}H NMR (400 MHz, d_6 -DMSO): δ 7.68 (s, 2H), 7.57 (d, J = 8 Hz, 2H), 6.97 (d, J = 8 Hz, 4H), 6.85 (d, J = 8 Hz, 4H), 6.66 (d, J = 8 Hz, 2H), 3.89 (t, J = 8 Hz, 4H),

1.70–1.63 (m, 4H), 1.42–1.36 (m, 4H), 1.30–1.26 (m, 8H), 0.85 (t, $J = 8$ Hz, 6H). ^{13}C NMR (400 MHz $CDCl_3$): δ 156.03, 150.073, 140.37, 135.87, 127.65, 118.08, 116.07, 68.30, 31.66, 29.37, 25.87, 14.53.

Synthesis of 4-(7-bromo-11,12-dibutoxy-1,4,5,8-tetrahydrodibenzo [a, c] phenazine-2-yl)-N,N-bis[4-(hexyloxy)phenyl]aniline (**10**). In a round bottomed flask 2,7 − dibromo-11,12 − dibutoxy-1,4,5,8 − tetrahydrodibenzo [a, c] phenazine (290 mg, 0.5 mmol) and (4-{bis[4-(hexyloxy)phenyl]amino} phenyl)boronic acid (200 mg, 0.4 mmol) were dissolved in 1,2-dimethoxyethane (15 mL). After that, to the flask [1,1′-bis(diphenylphosphino)ferrocene]dichloropalladium(II) (36 mg, 0.043 mmol) and aqueous potassium carbonate solution (1 M, 2 mL) were added. The content of the flask was heated up to boiling temperature and stirred overnight under argon atmosphere. After cooling water (60 mL) was added to the mixture and the solution was extracted with dichloromethane (3 × 20 mL). The combined organic phase was dried over sodium sulfate and evaporated under vacuum. The crude product was purified by column chromatography (toluene) on silica gel to afford a dark yellow solid (47% yield). ^{1}H NMR (400 MHz, $CDCl_3$): δ 9.37 (d, 1H), 9.31 (d, 1H), 8.35 (d, 1H), 8.25 (d, 1H), 7.84 (dd, 1H), 7.71 (dd, 1H), 7.69 (d, 2H), 7.39 (d, 2H), 7.14–7.10 (m, 4H), 7.08 (d, 2H), 6.88–6.84 (m, 4H), 4.24 (dt, 4H), 3.96 (d, 4H), 2.00–1.93 (m, 4H), 1.83–1.76 (m, 4H), 1.65–1.60 (m, 4H), 1.50–1.44 (m, 4H), 1.38–1.34 (m, 8H), 1.06 (dt, 6H), 0.92 (t, 6H). ^{13}C NMR (400 MHz $CDCl_3$): δ 155.80, 153.75, 148.75, 140.90, 140.50, 132.25, 132.13, 131.10, 127.95, 123.40, 123.28, 122.85, 121.95, 120.89, 115.57, 96.18, 68.54, 31.84, 31.18, 29.58, 26.00, 22.84, 19.54, 14.25, 14.14.

Synthesis of 4-[7-(4-{bis[4-(hexyl)phenyl]amino} phenyl)-11,12-dibutoxy-1,4,5,8-tetrahydrodibenzo [a, c] phenazine-2-yl]benzaldehyde (**11**). To a round bottomed flask 4-(7 − bromo-11,12 − dibutoxy-1,4,5,8-tetrahydrodibenzo [a, c] phenazine − 2 − yl)-N, N − bis[4-(hexyloxy)phenyl]aniline (378 mg, 0.4 mmol) and 4-formylphenyl boronic acid (68 mg, 0.4 mmol) were added and dissolved in 1,2-dimethoxyethane (15 mL). [1,1′-bis(diphenylphosphino)ferrocene]dichloropalladium(II) (33 mg, 0.04 mmol) and aqueous potassium carbonate solution (1 M, 2 mL) were added to the flask. The whole experimental set up was kept under argon atmosphere, heated up to boiling temperature, and stirred overnight. After that, the reaction mixture was mixed with water (60 mL) and extracted with dichloromethane (3 × 20 mL). The combined organic phase was dried over sodium sulfate and evaporated by rotary evaporator. The crude product was purified by column chromatography (dichloromethane/hexane: 1/1, v/v) on silica gel to yield a reddish orange solid (87% yield). ^{1}H NMR (400 MHz, $CDCl_3$): δ 10.04 (s, 1H), 9.30 (dd, 2H), 7.93–7.85 (m, 4H), 7.74 (d, 1H), 7.71 (t, 1H), 7.70–7.68 (m, 1H), 7.66 (d, 1H), 7.64 (s, 1H), 7.62 (s, 1H), 7.60 (t, 1H), 7.58 (t, 1H), 7.11 (d, 4H), 7.05 (d, 2H), 6.86 (m, 4H), 4.15 (t, 4H), 3.95 (t, 4H), 1.97–1.90 (m, 4H), 1.83–1.76 (m, 4H), 1.62–1.54 (m, 4H), 1.50–1.46 (m, 4H), 1.40–1.34 (m, 8H), 1.06 (t, 6H), 0.93 (t, 6H). ^{13}C NMR (400 MHz $CDCl_3$): δ 192.01, 155.85, 153.48, 140.87, 140.03, 135.40, 130.43, 129.20, 127.85, 127.55, 126.95, 123.48, 140.75, 115.60, 69.09, 68.55, 31.87, 31.25, 29.61, 26.03, 22.87, 19.59, 14.28, 14.18.

Synthesis of 5-[7-(4-{bis[4-(hexyloxy)phenyl]amino} phenyl)-11,12-dibutoxy-1,4, 5,8-tetrahydrodibenzo [a, c] phenazine-2-yl]thiophene-2-carbaldehyde (**12**). In a round bottomed flask a mixture of 4-(7 − bromo-11,12 − dibutoxy-1,4,5,8 − tetrahidrodibenzo [a, c] phenazine − 2 − yl)-N, N − bis[4-(hexyloxy)phenyl] aniline (378 mg, 0.4 mmol) and 5 − formyl − 2-thenylboronic acid (65 mg, 0.4 mmol) was dissolved in 1,2-dimethoxyethane. [1,1′-Bis(diphenylphosphino)ferrocene] dichloropalladium (II) (33 mg, 0.04 mmol) and aqueous potassium carbonate solution (1 M, 2 mL) were added to the flask. The whole content of the flask was refluxed under argon atmosphere overnight. The completion of the reaction was controlled by TLC. The reaction solution was mixed with water (60 mL) and extracted with dichloromethane (3 × 20 mL). Then the organic phase was dried over

sodium sulfate and evaporated by rotary evaporator. The crude product was purified by column chromatography (dichloromethane/hexane: 1/1, v/v) on silica gel to afford a red solid (85% yield). ^{1}H NMR (400 MHz, $CDCl_3$): δ 9.80 (s, 1H), 9.07 (d, 1H), 8.92 (d, 1H), 7.89–7.79 (m, 4H), 7.56–7.54 (m, 4H), 7.38–7.34 (m, 2H), 7.14–7.10 (m, 4H), 7.08–7.02 (t, 4H), 6.87 (d, 2H), 4.08 (t, 4H), 3.96 (t, 4H), 1.94–1.90 (m, 4H), 1.84–1.77 (m, 4H), 1.62–1.56 (m, 4H), 1.52–1.48 (m, 4H), 1.40–1.36 (m, 4H), 1.25 (t, 4H), 1.07 (t, 6H), 0.94 (t, 6H). ^{13}C NMR (400 MHz $CDCl_3$): δ 182.74, 155.85, 154.31, 153.36, 148.65, 142.21, 140.86, 139.85, 139.60, 137.40, 132.08, 130.92, 127.80, 126.98, 125.80, 124.53, 123.23, 120.63, 115.60, 106.73, 69.01, 68.56, 31.88, 31.30, 29.92, 29.62, 26.04, 22.87, 19.59, 14.29.

Synthesis of 3-{4-[7-(4-{bis[4-(hexyl)phenyl]amino} phenyl)-11,12-dibutoxy-1,4,5,8-tetrahydrodibenzo [a, c] phenazine-2-yl]phenyl} -2-cyano acrylic acid (**13**). To a round bottomed flask 4-[7-(4-{bis[4-(hexyloxy)phenyl] amino} phenyl)-11,12-dibutoxy-1,4,5,8-tetrahydrodibenzo [a, c] phenazine$-2-$yl]benzaldehyde (130 mg, 0.133 mmol) and cyano acetic acid (11 mg, 0.3 mmol) were added and dissolved in chloroform (15 mL). A catalytic amount of piperidine was added and the solution was refluxed under argon atmosphere overnight with stirring. After a TLC check, the reaction mixture was neutralized by 1 M aqueous hydrochloric acid solution and extracted with dichloromethane (3 $\times$ 20 mL) and water (3 $\times$ 20 mL). The combined organic phase was dried over sodium sulfate and the solvent was evaporated under vacuum. The crude product was purified by column chromatography (dichloromethane/hexane: 9.5/0.5, v/v) on silica gel to afford a red solid (90% yield). FT-IR (KBr pellet, cm$^{?1}$): 3398, 3028, 2954, 2934, 2850, 2336, 1716, 1594, 1504, 1284, 1240.

Synthesis of 3-{5-[7-(4-{bis[4-(hexyloxy)phenyl]amino} phenyl)-11,12-dibutoxy-1,4,5,8-tetrahydrodibenzo [a, c] phenazine-2-yl]-2-thienyl} -2-cyano acrylic acid (**14**). In a round bottomed flask 5-[7-(4-{bis[4-(hexyloxy) phenyl]amino} phenyl)-11,12$-$dibutoxy$-$1,4,5,8-tetrahydrodibenzo [a, c] phenazine$-2-$yl]thiophene$-2-$carbaldeyde (133 mg, 0.133 mmol) and cyanoacetic acid (11 mg, 0.13 mmol) were mixed and dissolved in chloroform (15 mL). A catalytic amount of piperidine was added to the solution in the flask, and then the content was stirred and refluxed under argon atmosphere overnight. Then the reaction mixture was neutralized by 1 M aqueous solution of hydrochloric acid and then extracted with dichloromethane (3 $\times$ 20 mL) and water (3 $\times$ 20 mL). The organic phases were separated, combined, dried over sodium sulfate, and finally the organic solvent was evaporated. The crude product was purified by column chromatography (dichloromethane/hexane: 9.5/0.5, v/v) to yield a dark red solid (89% yield). FT-IR (KBr pellet, cm^{-1}): 3420, 2956, 2926, 2852, 2362, 1716, 1588, 1506, 1282, 1240.

3.3. Photo-electrochemical device fabrication

The followed procedure for device fabrication was reported by Zafer et al.[11] FTO-coated glass substrates with the sheet resistance of 15 Ω/square, purchased from Solaronix, TEC15, were used for the device fabrication. TiO_2 was synthesized by sol-gel method and coated by screen printing technique on FTO substrates and dried at 70 °C in air. The active area of the TiO_2 coating was 1 cm^2. Substrates were sintered at 450 °C for 30 min in order to obtain the structure and the morphology of anatase TiO_2.[11] The thickness of the TiO_2 film was measured about 8 $\pm$ 0.5 μm by Ambiostech XP1 high resolution profilometer. After cooling down to 100 °C, the substrates were immersed into 5 $\times$ 10$^{?4}$ M KD-148 and KD-150 solutions in chloroform for 12 h at room temperature and then rinsed with acetonitrile. Counter electrodes were prepared by thermal reduction of Pt^{4+} to Pt^0. Next 1% hexachloroplatinic acid solution in 2-propanol was dropped on FTO substrates and burned at 450 °C for 10 min. Consequently, the sensitized TiO_2 electrode and Pt/FTO counter electrode were

assembled in sandwich geometry with a Surlyn gasket and iodide/triiodide redox couple containing electrolyte was injected into the cell through the pinhole predrilled in the counter electrode. The electrolyte consists of 0.6 M $1-$butyl-3-methyl imidazolium iodide, 0.1 M lithium iodide, 0.05 M iodine, and 0.5 M *tert*-butyl pyridine in $3-$methoxypropyonitrile.

3.4. Characterization

NMR spectra (^{1}H and ^{13}C) of all compounds synthesized in the content of this work were recorded at room temperature on a Bruker 400 MHz NMR spectrometer. Data are listed in parts per million (ppm) on delta scale (δ) and coupling constants are reported in Hz. The splitting patterns are designated as follows: s (singlet), d (doublet), t (triplet), q (quartet), and m (multiplet). IR was recorded on a PerkinElmer Spectrum BX. UV-Vis spectra of dyes were recorded on a Specord S600 diode array spectrophotometer at room temperature. PL spectra were recorded on an Edinburgh Instruments FLS920 spectrofluorometer in diluted chloroform solution (1×10^{-5} M).

Cyclic voltammetry analyses were carried out on a CH Instruments 660B Electrochemical Work Station at different scan rates in a three-electrode cell. The oxidation/reduction potentials of organic materials were measured in chloroform using a 0.1 M $TBAPF_6$ solution (in acetonitrile) as the supporting electrolyte, glassy carbon as working electrode, Ag/Ag^+ as reference electrode, and Pt wire as counter electrode. The system was calibrated with Fc/Fc^+ as an internal reference.

Prepared photo-electrochemical cells were characterized by current–voltage (I–V) measurement and measurement of incident photon-to-current-conversion-efficiency (IPCE) spectra in order to determine the photovoltaic performances. All I–V characteristics were obtained under white light illumination of 100 mW/cm^2 light intensity and AM 1.5 conditions by Keithley 2400 Source-Meter Unit and Labview data acquisition software. The solar simulator was calibrated with a reference Si solar cell calibrated at Fraunhofer ISE, Freiburg, Germany. The active area of the cells was adjusted to 1 cm^2 by black shadow mask to get rid of reflectance effects on the solar cell performance.

The overall energy conversion efficiency, η, was calculated using the equation

$$\eta = \frac{P_{\max}}{P_{\text{light}}} = \frac{V_{mpp} I_{mpp}}{P_{\text{light}}} = \frac{V_{oc} I_{sc} FF}{P_{\text{light}}},$$

where V_{oc} (V) is open circuit voltage, I_{sc} (mA/cm^2) is short circuit current, FF is fill factor, P_{max} (mW/cm^2) is maximum power point, P_{light} (mW/cm^2) is incident light power, and V_{mpp} and I_{mpp} are voltage and current at the point of maximum power output of the cell, respectively.[28]

The IPCEs were calculated using the following equation: IPCE [%] = 1240 $I_{sc}/(\lambda.I)$, where I_{sc} (mA/cm^2) is the short-circuit photocurrent density for monochromatic irradiation and λ (nm) and I (W/m^2) are the wavelength and the intensity of the monochromatic light. IPCE measurements were performed by Enlitec QE-R EQE/IQE measurement system.

4. Conclusions

In summary, we prepared organic push–pull dyes with high molar extinction coefficient consisting of a conjugated spacer of quinoxaline derivative, apart from the blocks of alkoxy substituted triphenylamine and cyanoacrylic acid anchoring functional moieties. On the basis of this study, we achieved photovoltaic conversion efficiencies

from DSSCs sensitized with KD-148 and KD-150 as 1.54% and 2.32%, respectively, where Z-907 yielded 4.07% conversion efficiency under 100 mW/cm^2 and AM 1.5G illumination. This achievement provided new information and new material as π-spacer to the literature on energy-level alignment and configuration of chromophores. More importantly, new quinoxaline derivatives were synthesized and attached from the phenantrene side to donor and acceptor groups as π-spacer with a weak acceptor property.

We think that new designs and developments of molecular structures and seeking optimum molecular alignment will lead to an improvement in device efficiencies.

Acknowledgment

We acknowledge the project support funds of the Ministry of Development of Turkey (11/DPT/001).

References

1. Oregan, B.; Gratzel, M. *Nature* **1991**, *353*, 737-740.
2. Gratzel, M. *Nature* **2001**, *414*, 338-344.
3. Gao, F.; Wang, Y.; Shi, D.; Zhang, J.; Wang, M. K.; Jing, X. Y.; Humphry-Baker, R.; Wang, P.; Zakeeruddin, S. M.; Gratzel, M. *J. Am. Chem. Soc.* **2008**, *130*, 10720-10728.
4. Yella, A.; Lee, H. W., Tsao, H. N.; Yi, C. Y.; Chandiran, A. K.; Nazeeruddin, M. K.; Diau, E. W. G.; Yeh, C. Y.; Zakeeruddin, S. M.; Gratzel, M. *Science* **2011**, *334*, 629-634.
5. Tanaka, H.; Takeichi, A.; Higuchi, K.; Motohiro, T.; Takata, M.; Hirota, N.; Nakajima, J.; Toyoda, T. *Sol. Energ. Mat. Sol. C.* **2009**, *93*, 1143-1148.
6. Akhtaruzzaman, M.; Mahmud, H. N. M. E.; Islam, A.; Shafei, A. E.; Karim, M. R.; Sopian, K.; Han, L. Y.; Yamamoto, Y. *Mater. Chem. Phys.* **2013**, *142*, 82-86.
7. Tang, J.; Qu, S. Y.; Hu, J.; Wu, W. J.; Hua, J. L. *Sol. Energy* **2012**, *86*, 2306-2311.
8. Wu, Q. P.; Xu, Y. J.; Cheng, X. B.; Liang, M.; Sun, Z.; Xue, S. *Sol. Energy* **2012**, *86*, 764-770.
9. Yang, C. H.; Lin, W. C.; Wang, T. L.; Shieh, Y. T.; Chen, W. J.; Liao, S. H.; Sun, Y. K. *Mater. Chem. Phys.* **2011**, *130*, 635-643.
10. Kandavelu, V.; Huang, H. S.; Jian, J. L.; Yang, T. C. K.; Wang, K. L.; Huang, S. T. *Sol. Energy* **2009**, *83*, 574-581.
11. Zafer, C.; Gultekin, B.; Ozsoy, C.; Tozlu, C.; Aydin, B.; Icli, S. *Sol. Energ. Mat. Sol. C.* **2010**, *94*, 655-661.
12. Im, M. J.; Park, J.; Gal, Y. S.; Moon, J. H.; Lee, J. Y.; Jin, S. H. *Mater. Chem. Phys.* **2013**, *139*, 319-326.
13. Zafer, C.; Kus, M.; Turkmen, G.; Dincalp, H.; Demic, S.; Kuban, B.; Teoman, Y.; Icli, S. *Sol. Energ. Mat. Sol. C* **2007**, *91*, 427-431.
14. Yang, J. B.; Ganesan, P.; Teuscher, J.; Moehl, T.; Kim, Y. J.; Yi, C. Y.; Comte, P.; Pei, K.; Holcombe, T. W.; Nazeeruddin, M. K.; et al. *J. Am. Chem. Soc.* **2014**, *136*, 5722-5730.
15. Stephan, M.; Zupancic, B.; Mohar, B. *Tetrahedron* **2011**, *67*, 6308-6315.
16. Antonisse, M. M. G.; Snellink-Ruel, B. H. M.; Yigit, I.; Engbersen, J. F. J.; Reinhoudt, D. N. *J. Org. Chem.* **1997**, *62*, 9034-9038.
17. Ma, T.; Zhang, S. J., Li, Y. F.; Yang, F. C.; Gong, C. L.; Zhao, J. *J. Polym. Degrad. Stabil.* **2010**, *95*, 1244-1250.
18. Chang, D. W.; Lee, H. J.; Kim, J. H.; Park, S. Y.; Park, S. M.; Dai, L.; Baek, J. B. *Org. Lett.* **2011**, *13*, 3880-3883.
19. Shklover, V.; Ovchinnikov, Y. E.; Braginsky, L. S.; Zakeeruddin, S. M.; Gratzel, *M. Chem. Mater.* **1998**, *10*, 2533-2541.
20. Kajzar, F.; Prasad, P. In *Organic Molecules for Nonlinear Optics and Photonics;* Morley, J. O.; Pavlides, P.; Pugh, J. Messier, D., Springer: Dordrecht, Netherlands, 1991, pp. 37-52.

21. Wu, I. Y.; Lin, J. T.; Luo, J.; Li, C. S.; Tsai, C.; Wen, Y. S.; Hsu, C. C.; Yeh, F. F.; Liou, S. *Organometallics* **1998**, *17*, 2188-2198.

22. March, J. *Advanced Organic Chemistry: Reactions, Mechanisms, and Structure*; Wiley: Hoboken, NJ, USA, 1992.

23. Caspar, J. V.; Meyer, T. J. *J. Am. Chem. Soc.* **1983**, *105*, 5583-5590.

24. Guo, K. P.; Yan, K. Y.; Lu, X. Q.; Qiu, Y. C.; Liu, Z. K.; Sun, J. W.; Yan, F.; Guo, W. Y.; Yang, S. H. *Org. Lett.* **2012**, *14*, 2214-2217.

25. Kroeze, J. E.; Hirata, N.; Koops, S.; Nazeeruddin, M. K.; Schmidt-Mende, L.; Graetzel, M; Durrant, J. R. *J. Am. Chem. Soc.* **2006**, *128*, 16376-16383.

26. Yu, Q. Y.; Liao, J. Y.; Zhou, S. M.; Shen, Y.; Liu, J. M.; Kuang, D. B.; Su, C. Y. *J. Phys. Chem. C* **2011**, *115*, 22002-22008.

27. Wan, Z.; Jia, C.; Wang, Y.; Yao, X. *RSC Adv.* **2015**, 5, 50813-50820.

28. Neamen, D. A. *Semiconductor Physics and Devices: Basic Principles*; McGraw-Hill; New York, NY, USA, 2011.

Supporting Data

Supporting Information: NMR and FT-IR spectra of the synthesized materials are in the supporting information part.

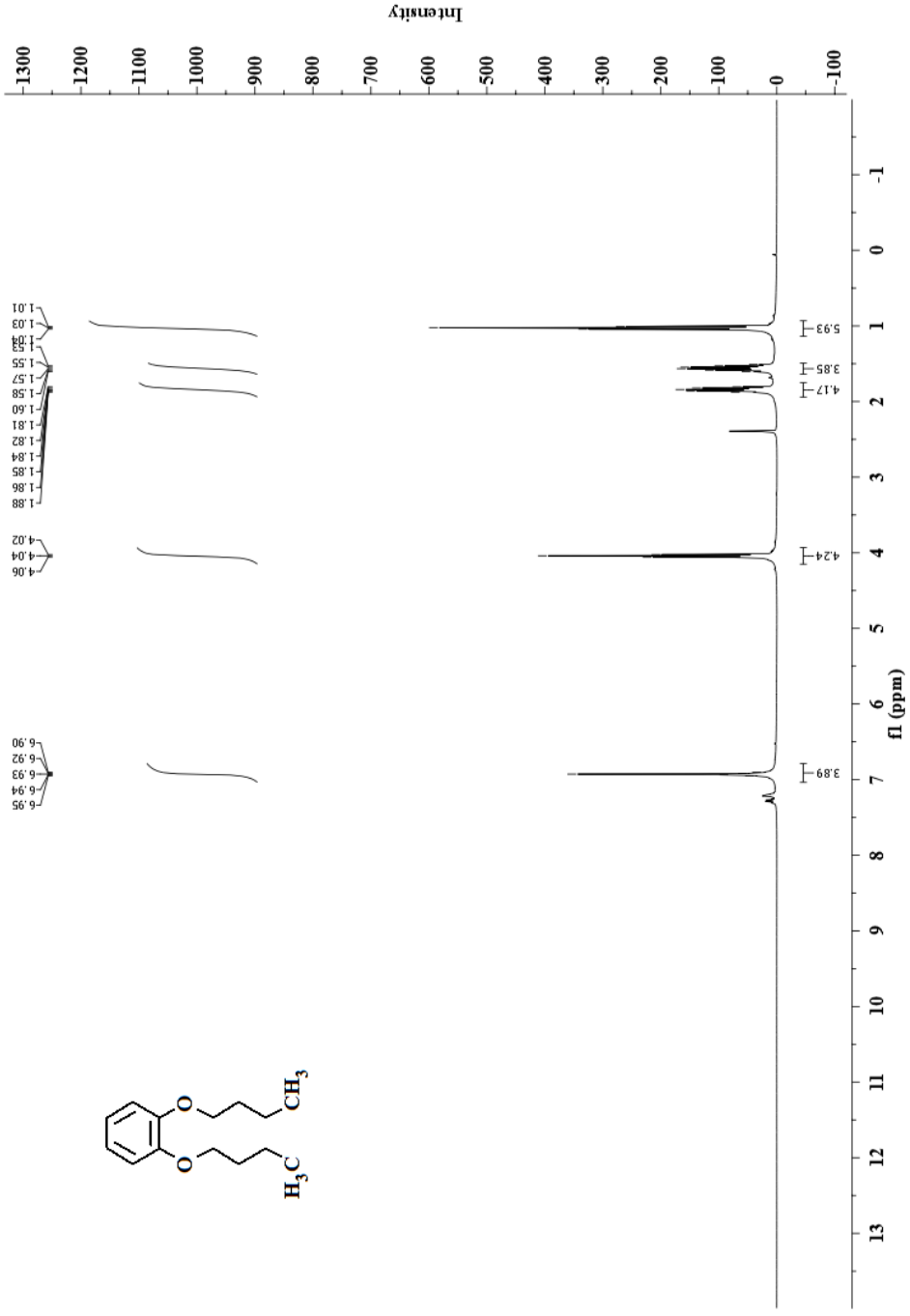

Figure S1. ^{1}H NMR spectra of Intermediate **2** recorded in d6-DMSO.

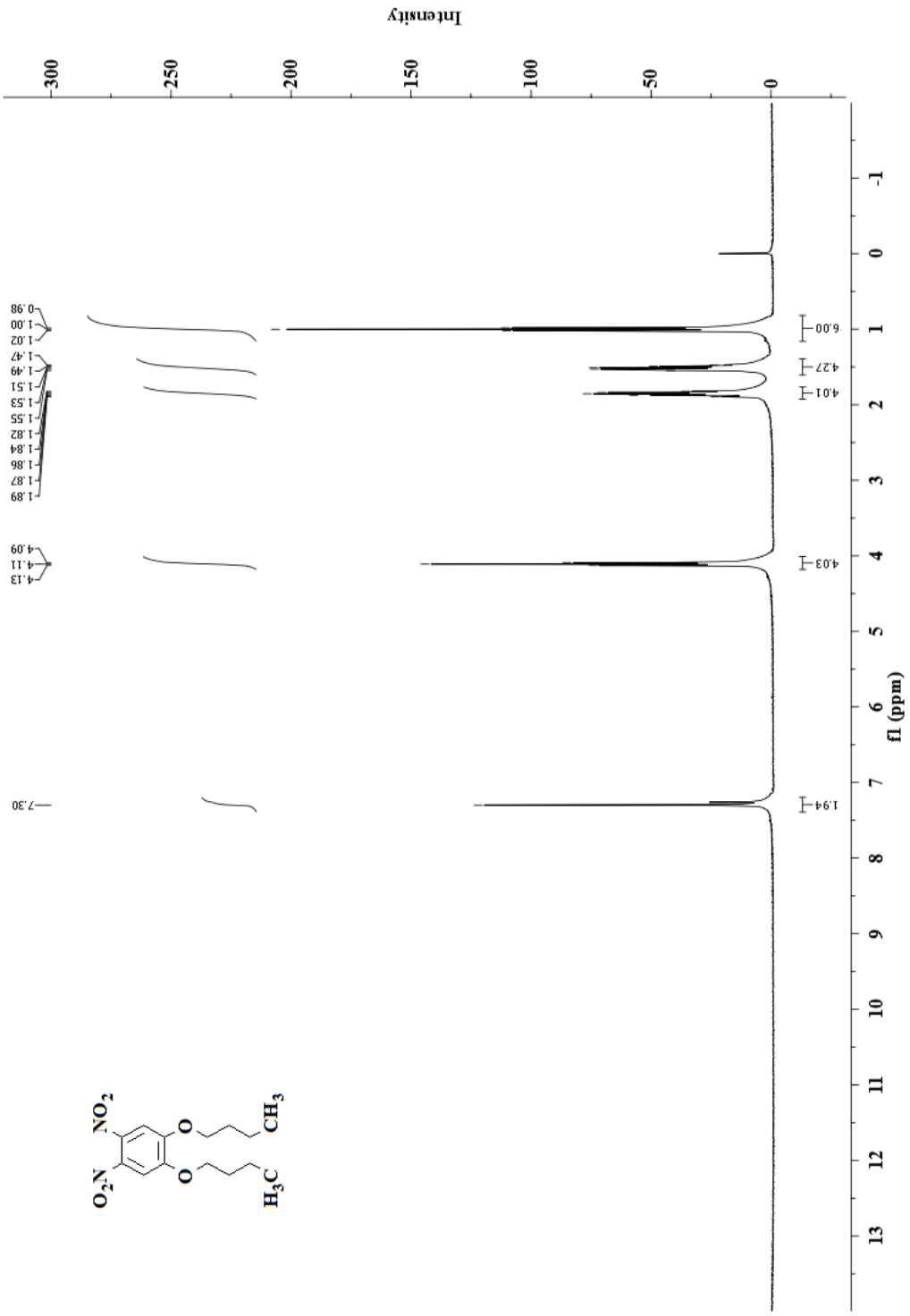

Figure S2. ^{1}H NMR spectra of Intermediate **3** recorded in $CDCl_3$.

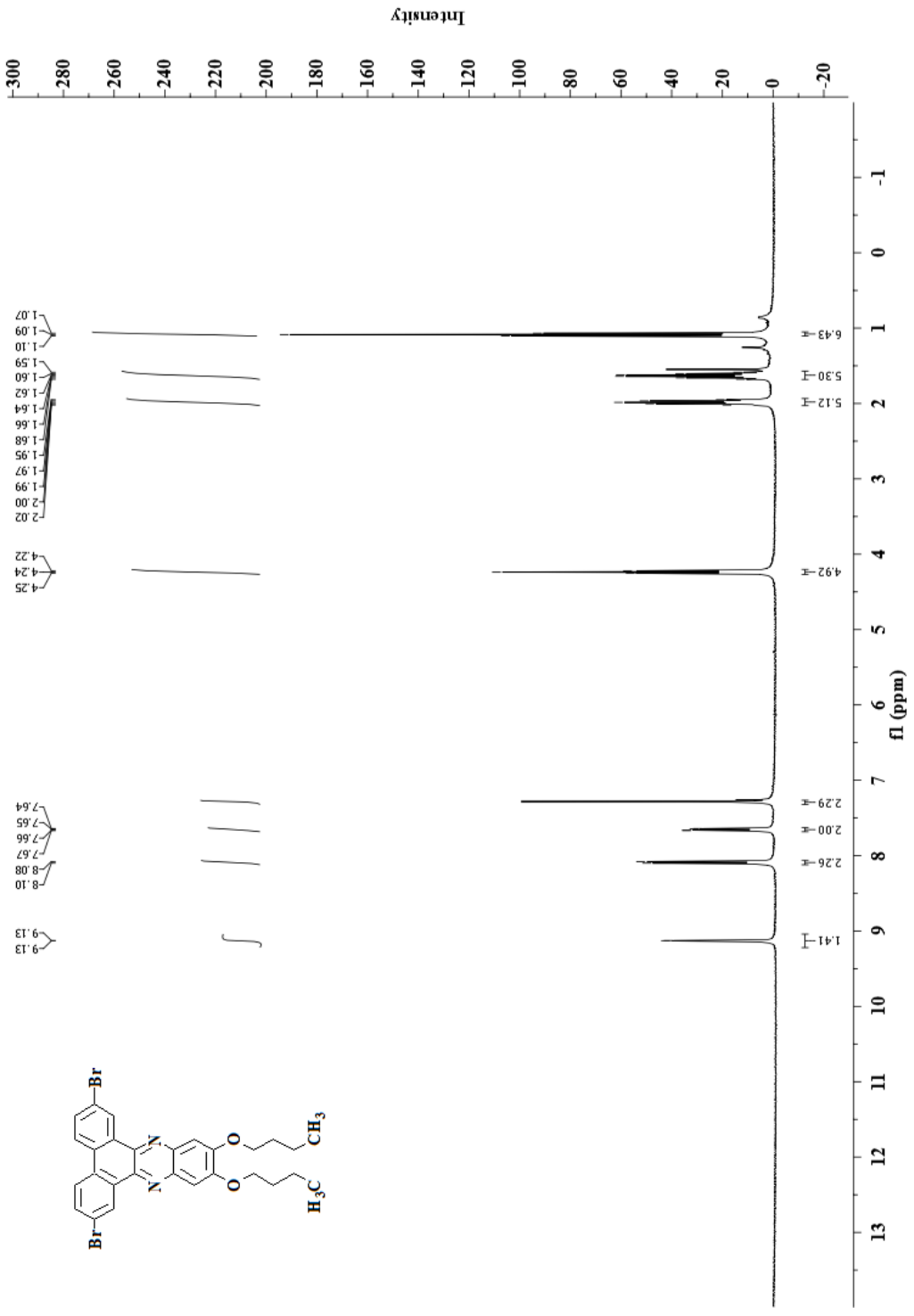

Figure S3. ^{1}H NMR spectra of Intermediate **5** recorded in $CDCl_3$.

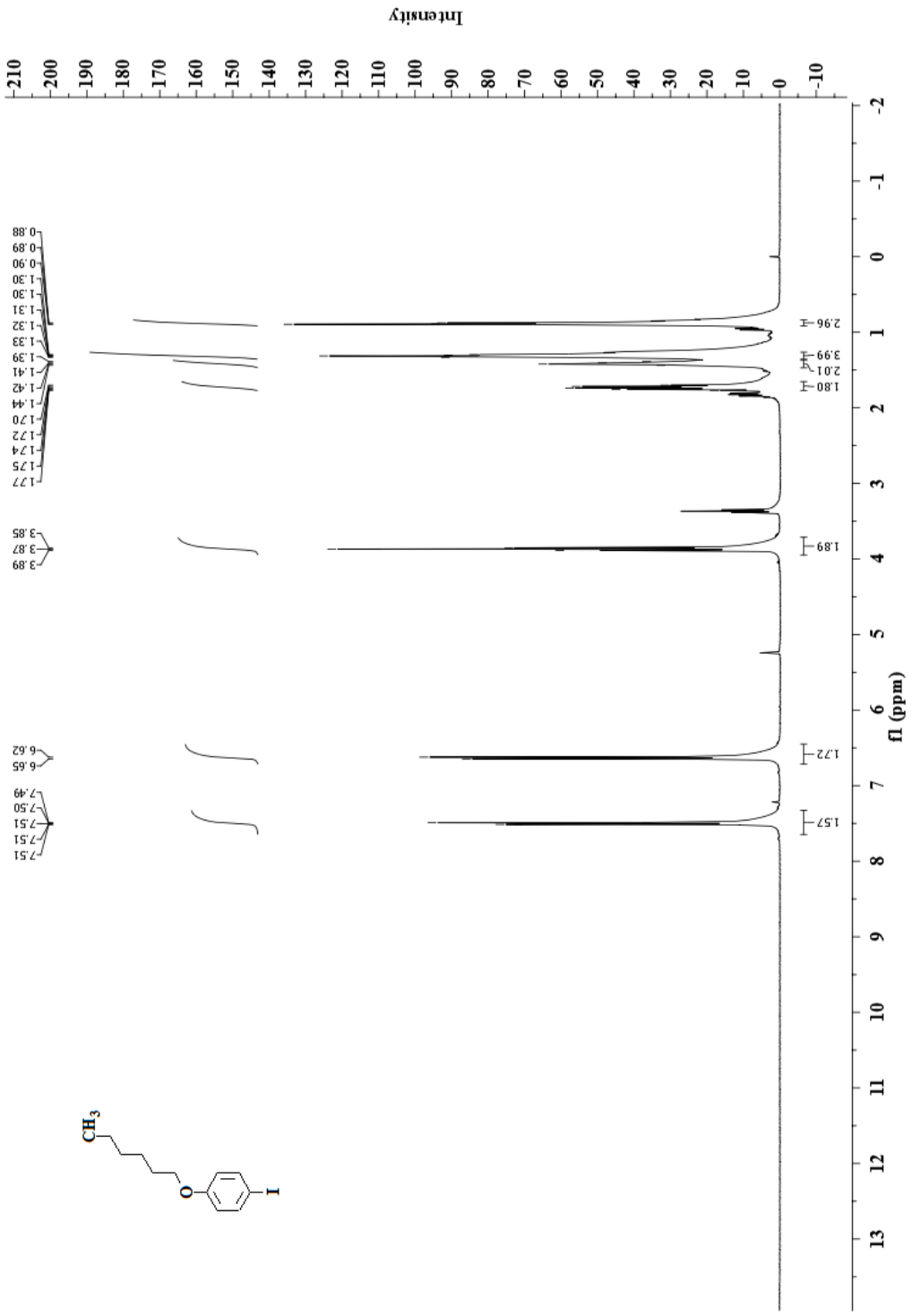

Figure S4. ^{1}H NMR spectra of Intermediate **7** recorded in $CDCl_3$.

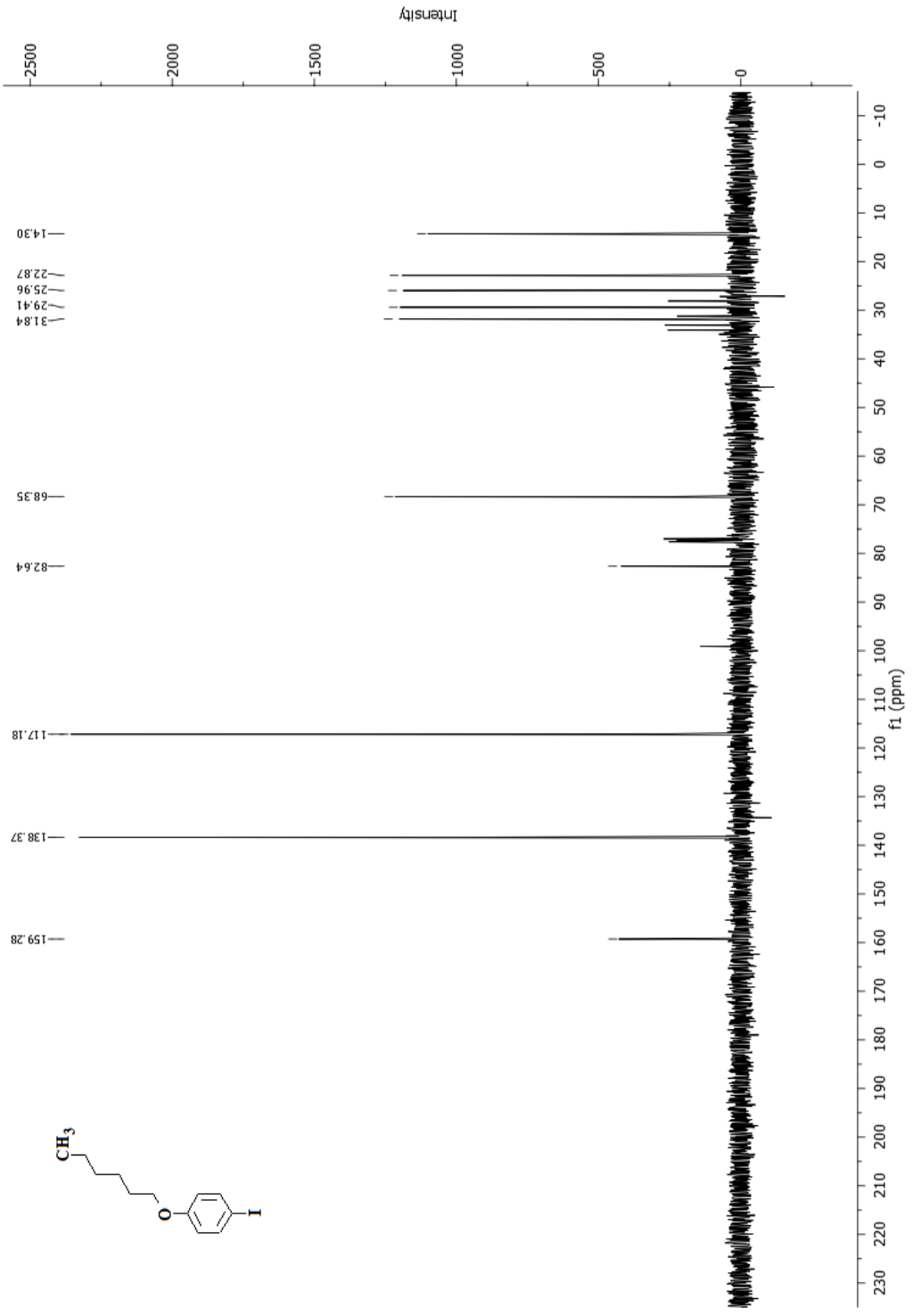

Figure S5. ^{13}C NMR spectra of Intermediate **7** recorded in $CDCl_3$.

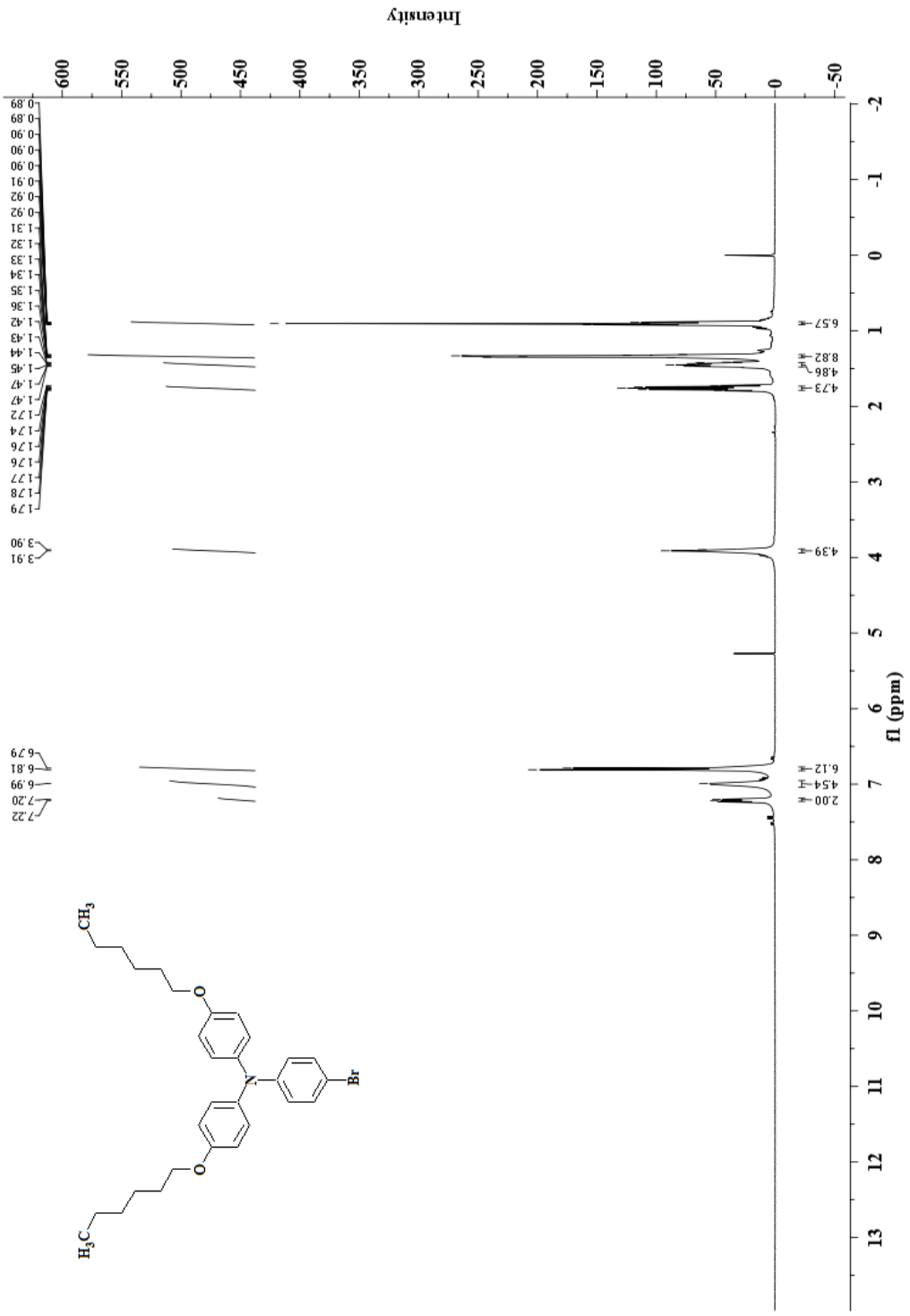

Figure S6. ^{1}H NMR spectra of Intermediate **8** recorded in $CDCl_3$.

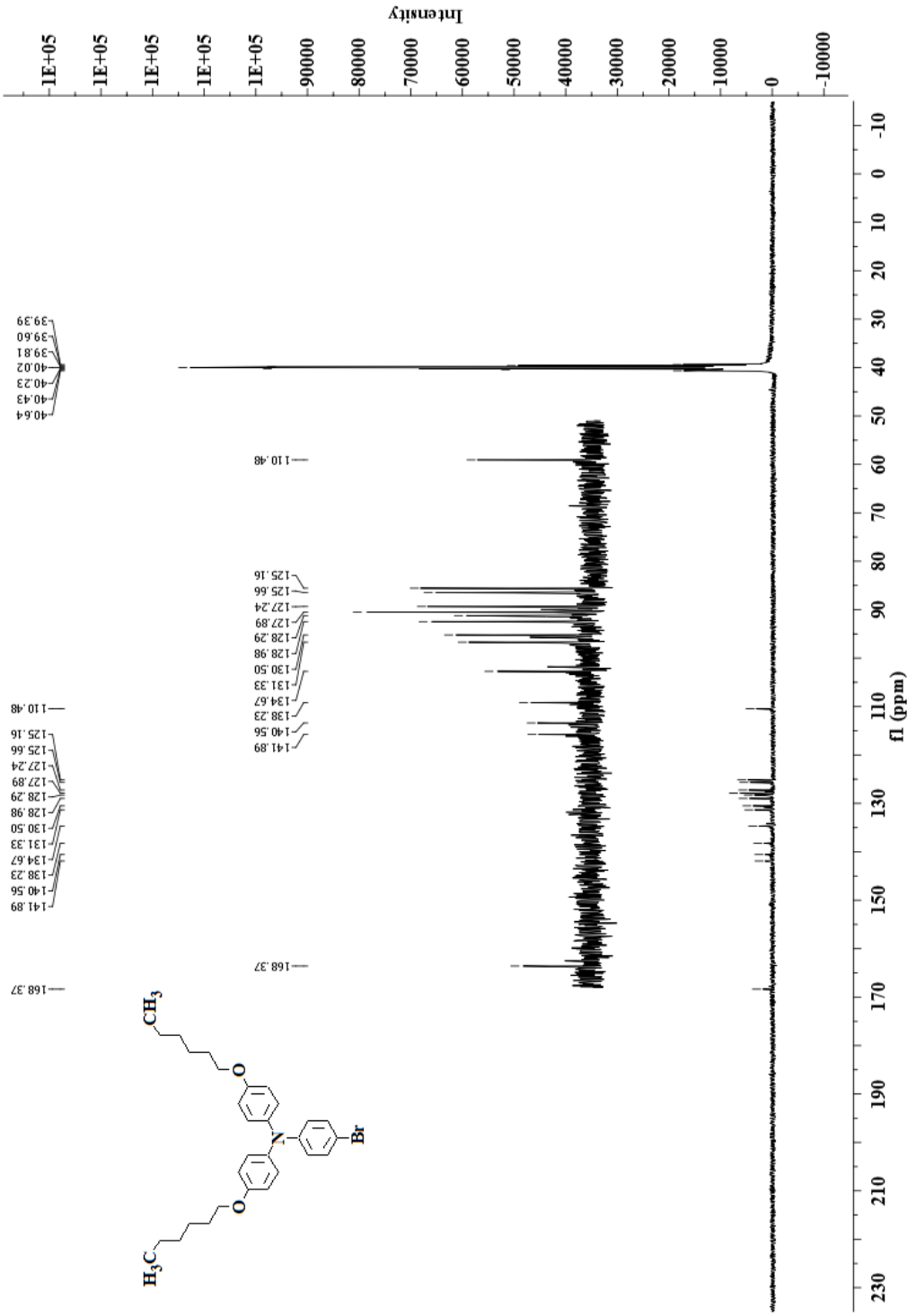

Figure S7. ^{13}C NMR spectra of Intermediate **8** recorded in $CDCl_3$.

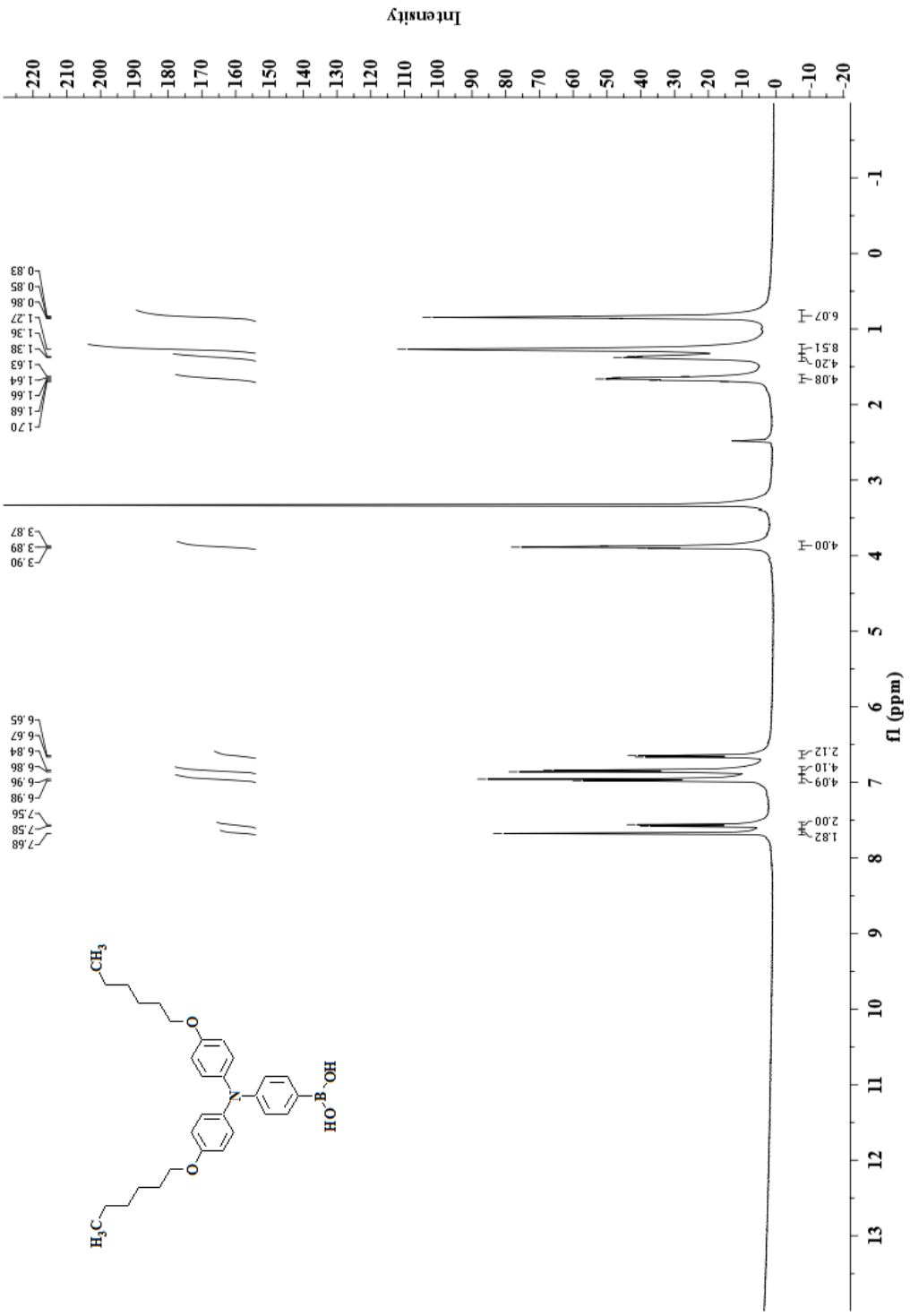

Figure S7. ^{1}H NMR spectra of Intermediate **9** recorded in d6-DMSO.

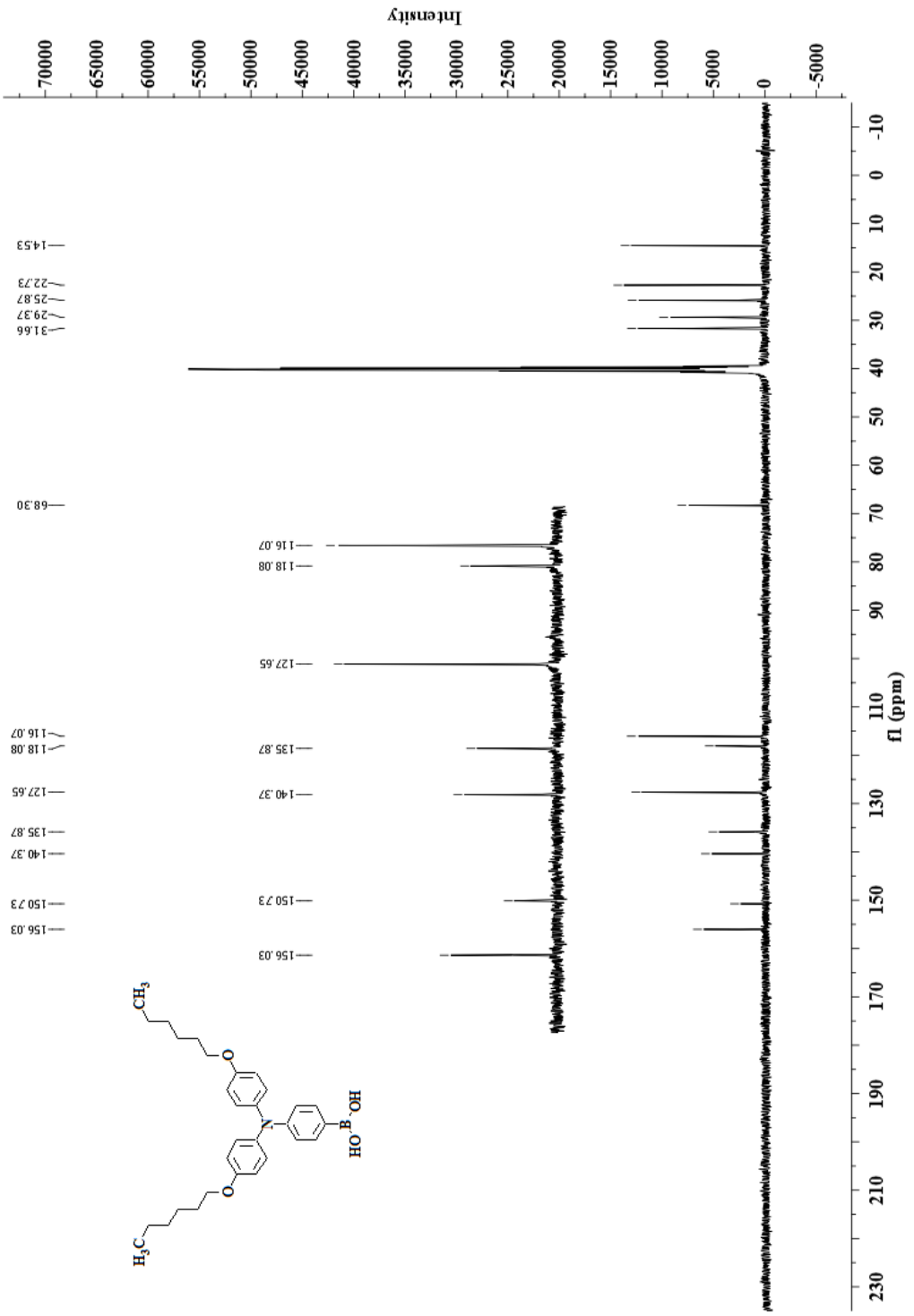

Figure S8. ^{13}C NMR spectra of Intermediate **9** recorded in d6-DMSO.

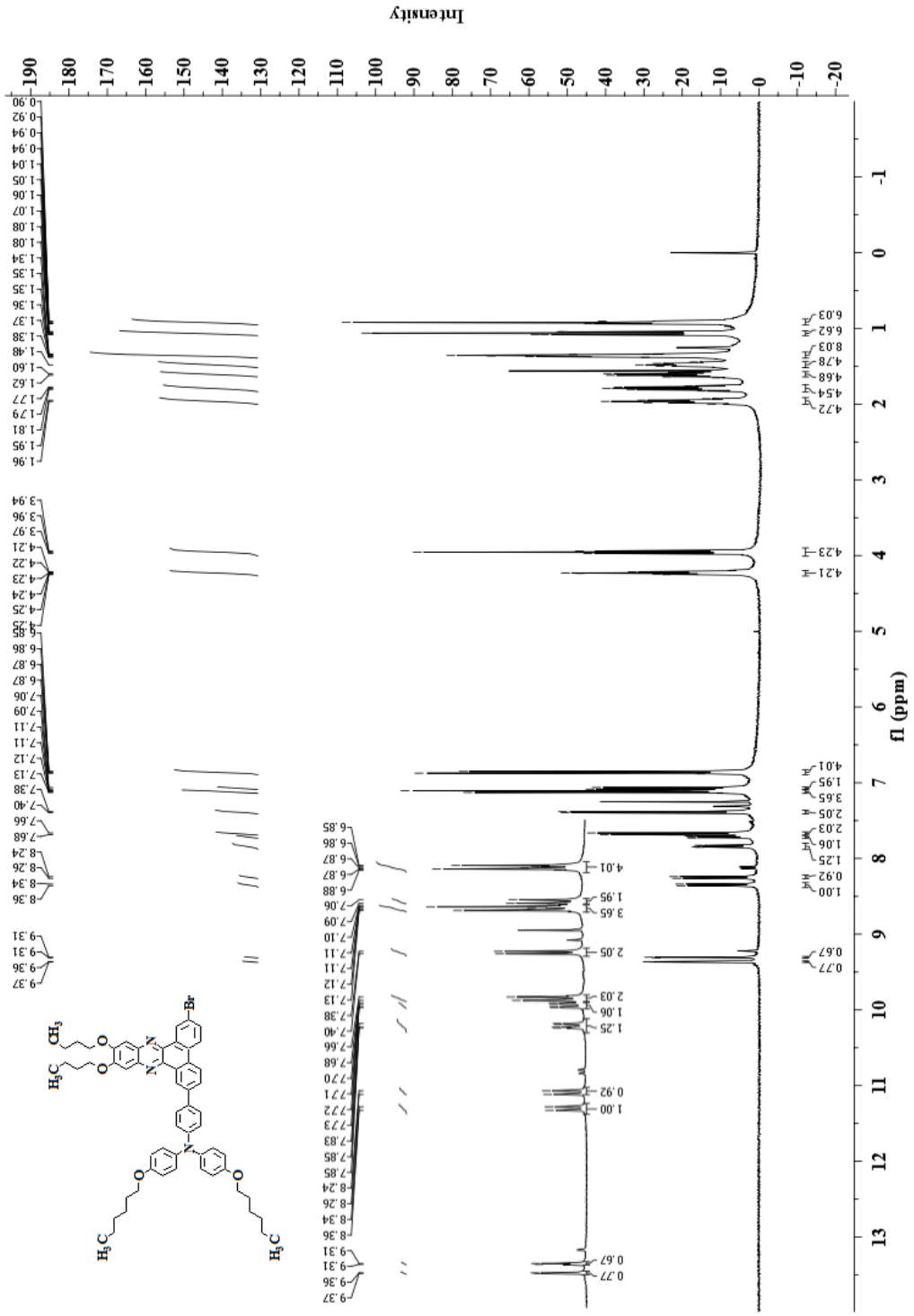

Figure S9. ^{1}H NMR spectra of Intermediate **10** recorded in $CDCl_3$.

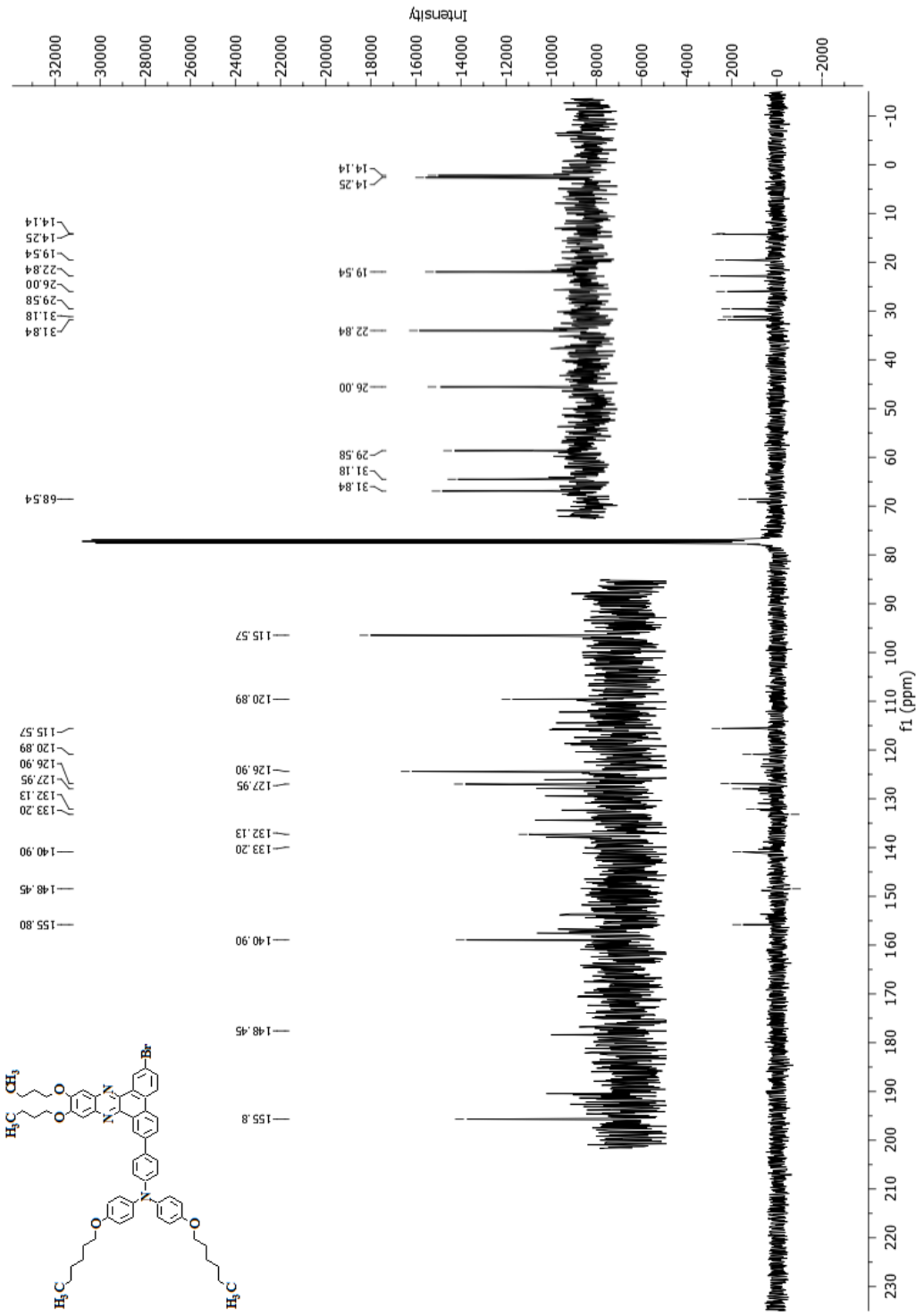

Figure S10. ^{13}C NMR spectra of Intermediate **10** recorded in $CDCl_3$.

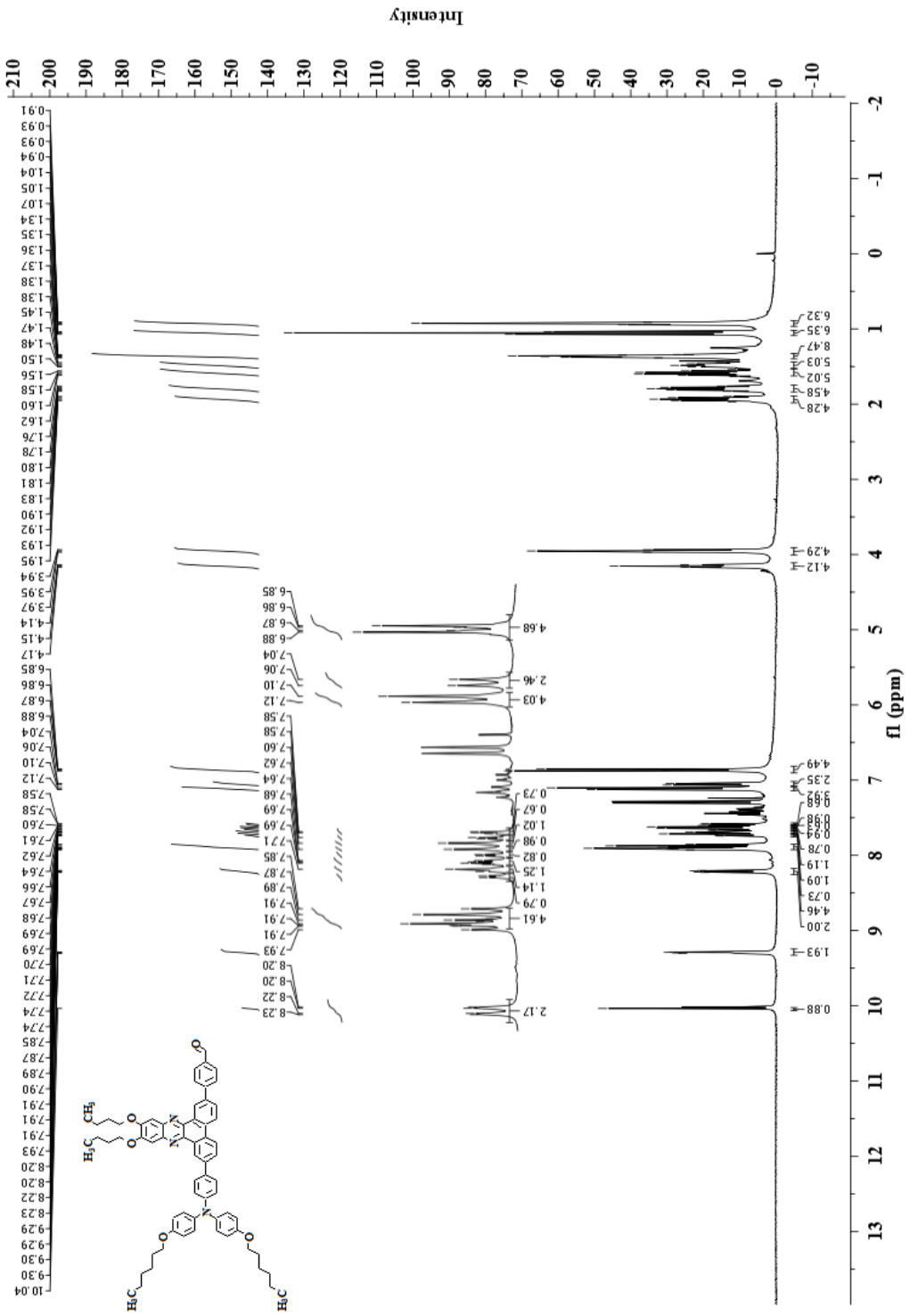

Figure S11. ^{1}H NMR spectra of Intermediate **11** recorded in $CDCl_3$.

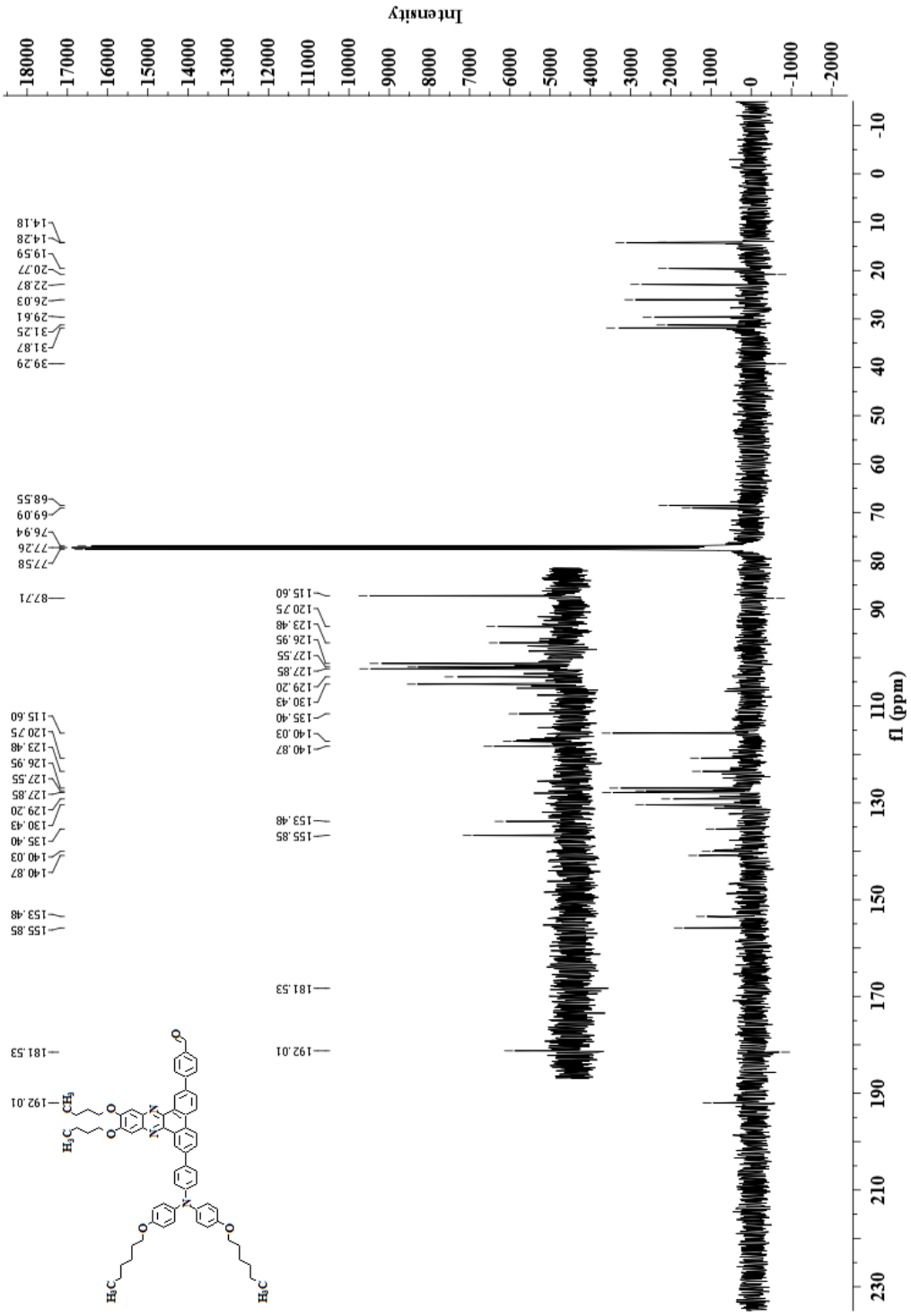

Figure S12. ^{13}C NMR spectra of Intermediate **11** recorded in $CDCl_3$.

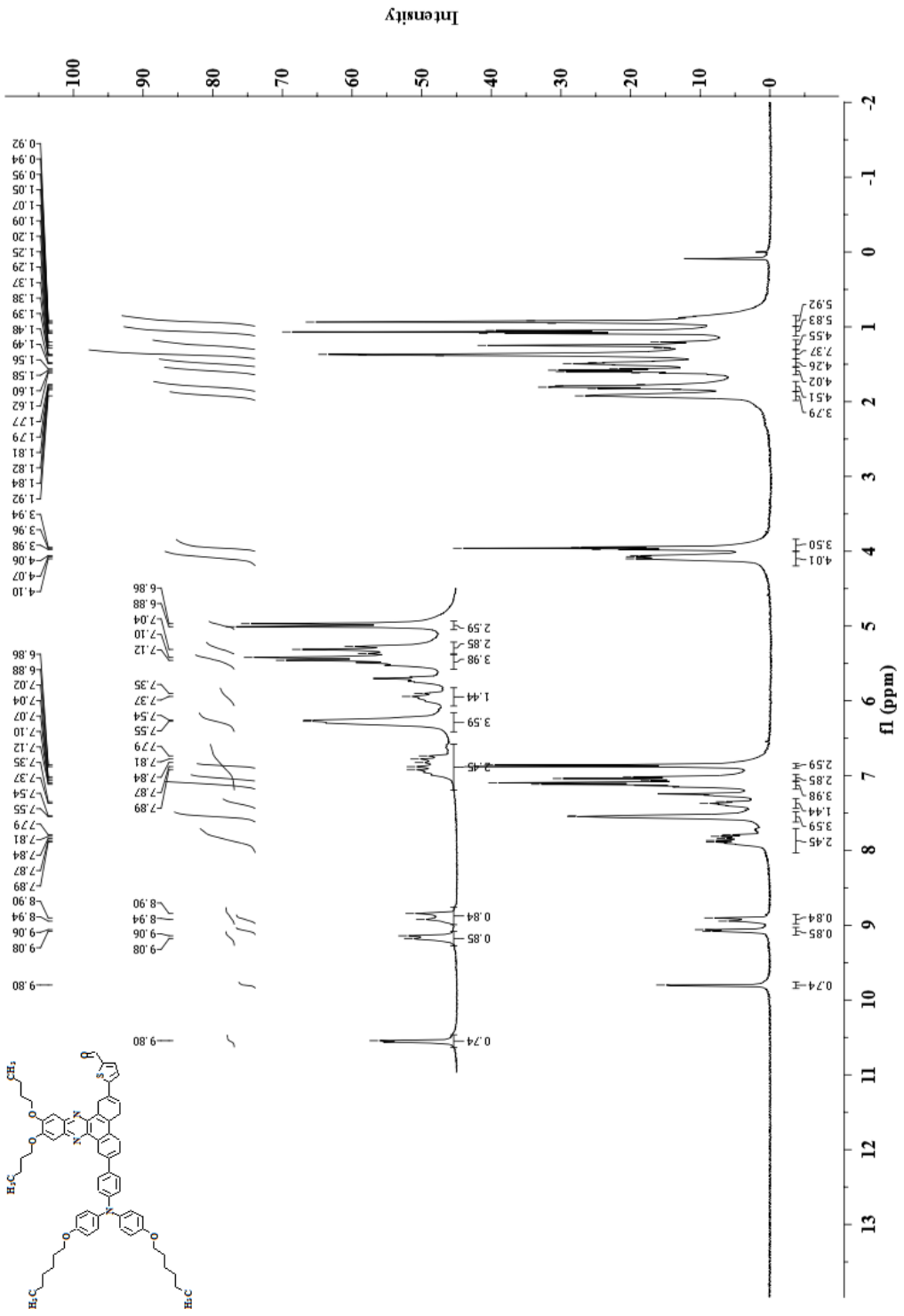

Figure S11. ^{1}H NMR spectra of Intermediate **12** recorded in $CDCl_3$.

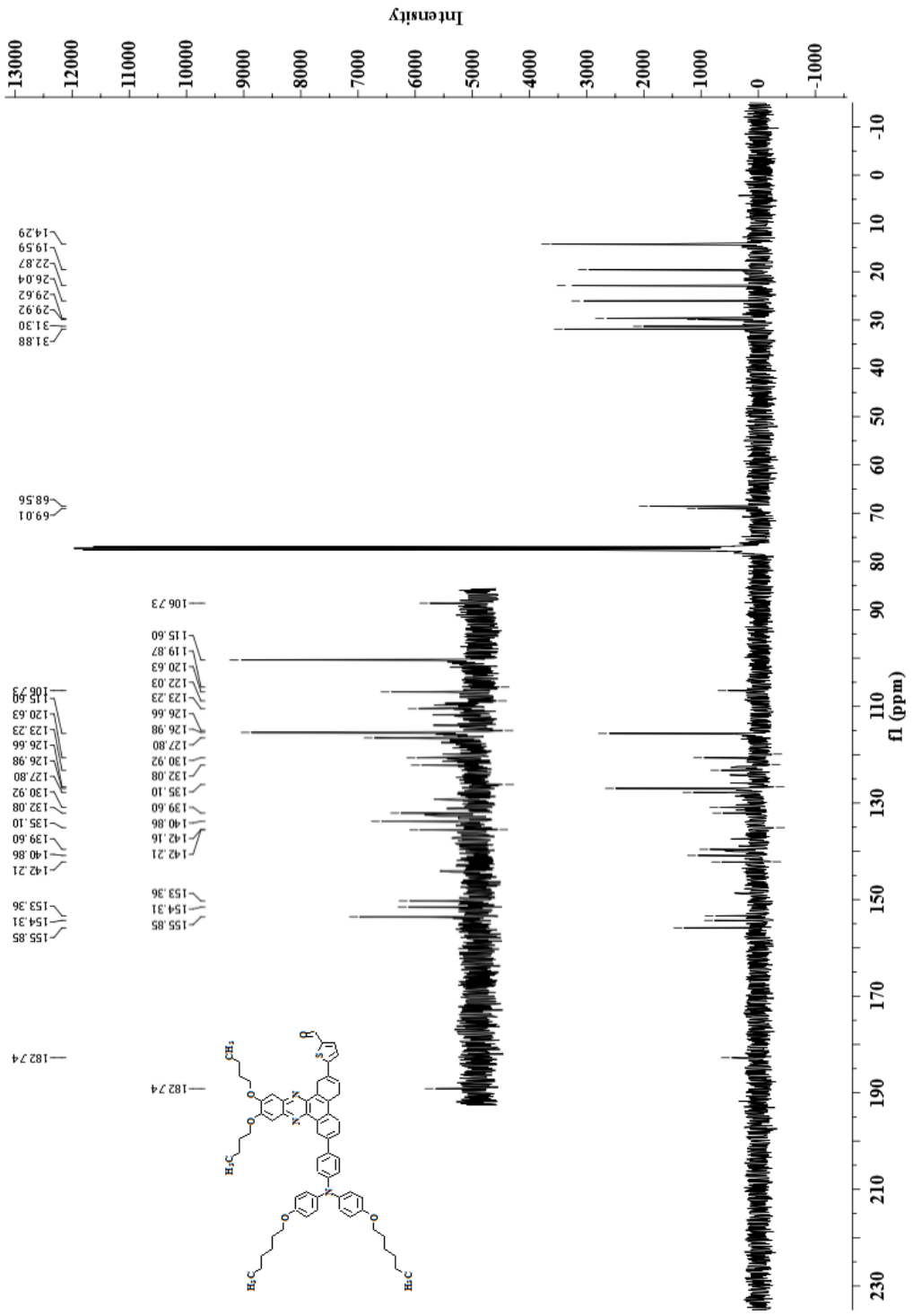

Figure S12. ^{13}C NMR spectra of Intermediate **12** recorded in $CDCl_3$.

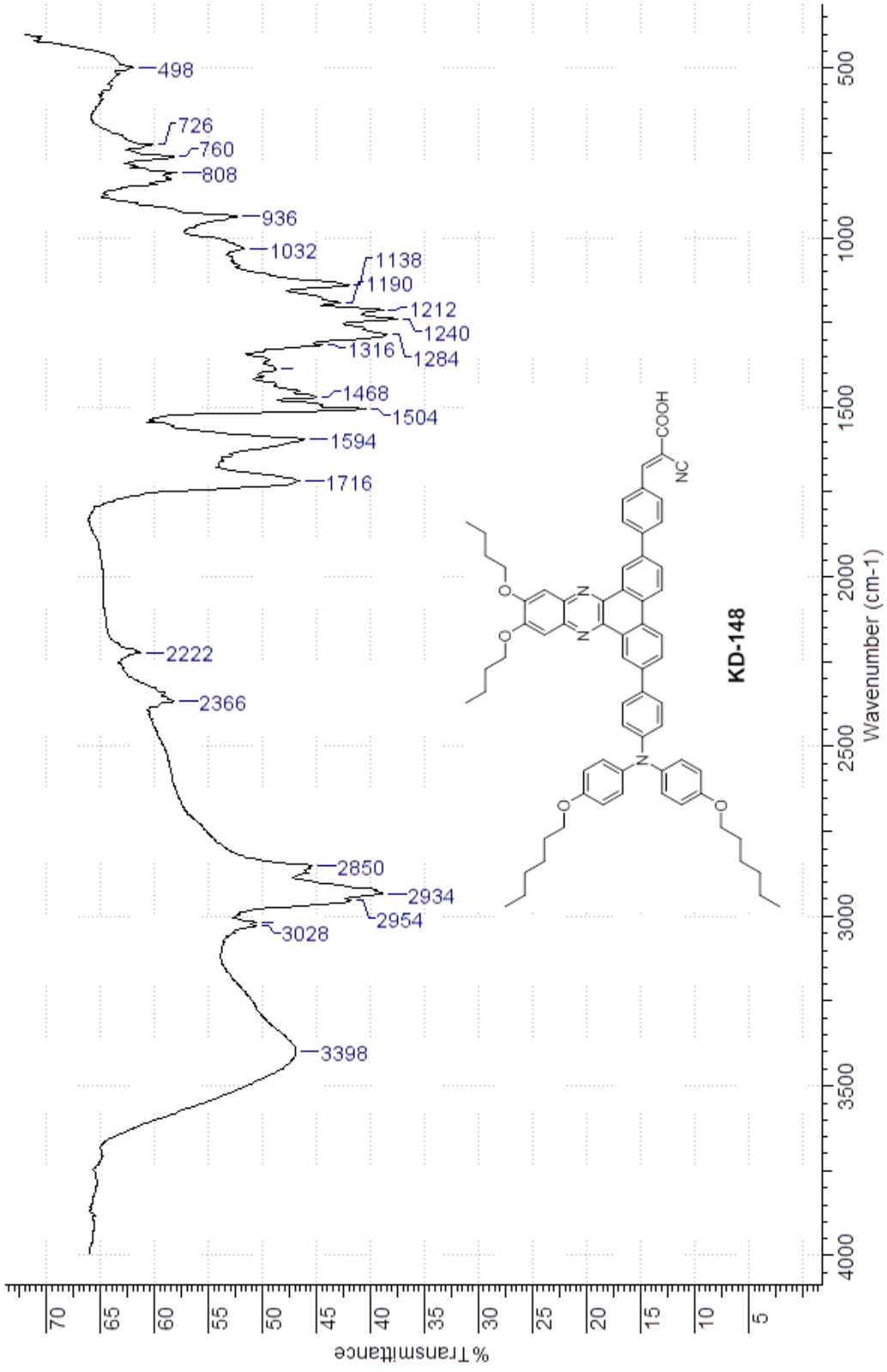

Figure S13. FT-IR spectra of Final Product **13**.

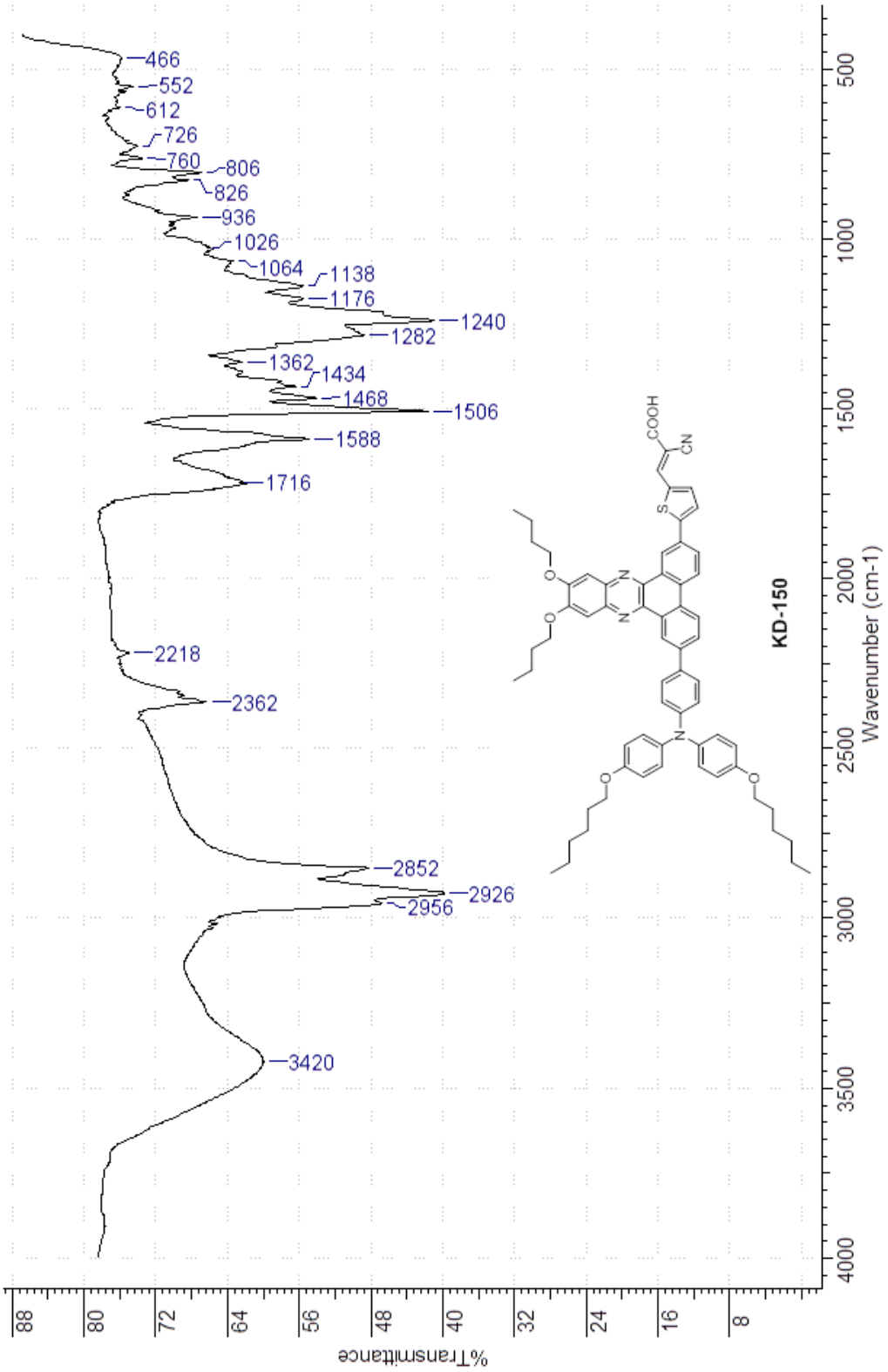

Figure S14. FT-IR spectra of Final Product **14**.